
Since January 2020 Elsevier has created a COVID-19 resource centre with free information in English and Mandarin on the novel coronavirus COVID-19. The COVID-19 resource centre is hosted on Elsevier Connect, the company's public news and information website.

Virology 508 (2017) 134–149

Contents lists available at ScienceDirect

Virology

journal homepage: www.elsevier.com/locate/yviro

# Glutamine antagonist-mediated immune suppression decreases pathology but delays virus clearance in mice during nonfatal alphavirus encephalomyelitis

Victoria K. Baxter[a,b,1], Rebecca Glowinski[a], Alicia M. Braxton[a], Michelle C. Potter[c,2], Barbara S. Slusher[c], Diane E. Griffin[a,*]

[a] W. Harry Feinstone Department of Molecular Microbiology and Immunology, Johns Hopkins Bloomberg School of Public Health, Baltimore, MD 21205, USA
[b] Department of Molecular and Comparative Pathobiology, Johns Hopkins University School of Medicine, Baltimore, MD 21205, USA
[c] Johns Hopkins Drug Discovery and Department of Neurology, Johns Hopkins University School of Medicine, Baltimore, MD 21205, USA

ARTICLE INFO

*Keywords:*
Alphavirus encephalomyelitis
Sindbis virus
6-diazo-5-oxo-l-norleucine
Viral pathogenesis
Immune response
Glutamate excitotoxicity

ABSTRACT

Infection of weanling C57BL/6 mice with the TE strain of Sindbis virus (SINV) causes nonfatal encephalomyelitis associated with hippocampal-based memory impairment that is partially prevented by treatment with 6-diazo-5-oxo-l-norleucine (DON), a glutamine antagonist (Potter et al., J Neurovirol 21:159, 2015). To determine the mechanism(s) of protection, lymph node and central nervous system (CNS) tissues from SINV-infected mice treated daily for 1 week with low (0.3 mg/kg) or high (0.6 mg/kg) dose DON were examined. DON treatment suppressed lymphocyte proliferation in cervical lymph nodes resulting in reduced CNS immune cell infiltration, inflammation, and cell death compared to untreated SINV-infected mice. Production of SINV-specific antibody and interferon-gamma were also impaired by DON treatment with a delay in virus clearance. Cessation of treatment allowed activation of the antiviral immune response and viral clearance, but revived CNS pathology, demonstrating the ability of the immune response to mediate both CNS damage and virus clearance.

## 1. Introduction

Recent epidemics of rash, arthritis and encephalomyelitis emphasize the importance of arthropod-borne viruses, primarily alphaviruses and flaviviruses, to threaten public health (Lubelczyk et al., 2013; ; Molaei et al., 2015; Weaver et al., 1996). Encephalomyelitis induced by infection with alphaviruses can be severe, with outcome dependent on the virus species (Babi et al., 2014; Baig et al., 2014; Bruyn and Lennette, 1953; Ethier and Rogg, 2012; Harvala et al., 2009; Lury and Castillo, 2004; Mancao et al., 2009; Przelomski et al., 1988; Reddy et al., 2008; Rivas et al., 1997; Rozdilsky et al., 1968; Schultz et al., 1977; Vilcarromero et al., 2010). Eastern equine encephalitis virus is most neurovirulent with fatalities most commonly in infants and children and frequent neurologic sequelae in those that survive (Deresiewicz et al., 1997; Finley et al., 1955). Currently, no treatments beyond supportive care are available, and no licensed vaccines for alphavirus encephalomyelitis are approved for non-military human use, so there is a need to identify new approaches to treatment (Go et al., 2014).

Infection of mice with Sindbis virus (SINV) leads to encephalomyelitis, providing a model for evaluating clinical disease and central nervous system (CNS) pathology induced by alphavirus infection. SINV preferentially infects neurons in mice, particularly the hippocampal neurons of the brain and the motor neurons of the spinal cord, and outcome is dependent on the strain of infecting virus and genetic background of the mouse (Kimura and Griffin, 2003; Griffin, 2011). Weanling C57BL/6 mice infected with the neurovirulent NSV strain of SINV develop fatal encephalomyelitis while mice infected with the less virulent TE strain recover with persistent hippocampal-dependent memory deficits as measured by fear conditioning (Jackson et al., 1988; Potter et al., 2015).

The immune response to alphavirus infection of the CNS presents a

* Correspondence to: Mailing address: Molecular Microbiology and Immunology, Johns Hopkins Bloomberg School of Public Health, 615 N. Wolfe St, Rm E5636, Baltimore, MD 21205, USA.
*E-mail addresses:* vkbaxter@med.unc.edu (V.K. Baxter), rglowin1@jhu.edu (R. Glowinski), abraxto6@jhmi.edu (A.M. Braxton), michelle.potter@merck.com (M.C. Potter), bslusher@jhmi.edu (B.S. Slusher), dgriffi6@jhu.edu (D.E. Griffin).
[1] Present Address: Department of Pathology and Laboratory Medicine, University of North Carolina at Chapel Hill, Chapel Hill, NC, USA 27599.
[2] Present Address: Merck Research Laboratories, 33 Avenue Louis Pasteur, Boston, MA, USA 02115.

http://dx.doi.org/10.1016/j.virol.2017.05.013
Received 11 April 2017; Received in revised form 14 May 2017; Accepted 17 May 2017
Available online 19 May 2017
0042-6822/ 

double-edged sword: while the immune response is necessary for bringing virus replication and production under control, it is also responsible for many of the pathological changes and neurological damage produced. After infection with the neurovirulent NSV strain of SINV, fatal encephalomyelitis coincides with infiltration of $CD4^+$ and $CD8^+$ T cells into the brain (Kulcsar et al., 2014), and in studies of mice lacking components of the immune response, particularly T cell deficits, mortality and severity of disease are decreased (Rowell and Griffin, 2002; Kimura and Griffin, 2003). Furthermore, previous studies have shown that inhibition of the immune response and glutamate excitotoxicity with 2-amino-3-(5-methyl-3-oxo-1,2-oxazol-4-yl) propranoic acid (AMPA) receptor antagonists can protect NSV-infected mice from fatal encephalomyelitis (Greene et al., 2008; Nargi-Aizenman et al., 2004).

DON is a diazo-containing glutamine analog that acts as a broad irreversible competitive inhibitor of several glutamine-utilizing enzymes (Thangavelu et al., 2014). During growth and proliferation, T cells preferentially use glutamine instead of glucose as an energy source, and rapidly dividing activated T cells show increased glutamine uptake and metabolism (Carr et al., 2010; Maciolek et al., 2014). Therefore, glutamine antagonism can inhibit lymphocyte proliferation (Wang et al., 2011). In the CNS, the excitatory neurotransmitter glutamate is synthesized from glutamine by the amidohydrolase enzyme glutaminase. Excess production of glutamate leads to neuronal death through glutamate excitotoxicity, so inhibition of glutaminase via DON might abrogate this process (Sattler and Tymianski, 2001). In support of this approach, mice infected with the fatal NSV strain of SINV show reduced mortality with DON treatment (Manivannan et al., 2016), and in the less virulent TE strain of SINV, DON reduces the development of clinical disease and hippocampus-dependent memory deficits (Potter et al., 2015). To determine the mechanism(s) by which DON improves outcome from nonfatal alphavirus encephalomyelitis, we have examined the effect of treatment on both pathological changes and virus clearance in the CNS.

## 2. Materials and methods

### 2.1. Sindbis virus infection and DON administration

The TE strain of SINV (Lustig et al., 1988) was grown and assayed by plaque formation in baby hamster kidney (BHK) cells. Four to six-week-old male C57BL/6 mice (Jackson Laboratory) were infected intranasally with $10^5$ pfu SINV in 20 μL PBS or mock-infected with 20 μL PBS while under light isoflurane anesthesia. DON was intraperitoneally administered once a day from the day of infection to 7 days post infection (DPI) at a dose of 0.3 mg/kg (low dose) or 0.6 mg/kg (high dose) as previously described (Potter et al., 2015). Control animals received the same volume of PBS. All studies were done in accordance with protocols approved by the Johns Hopkins University Institutional Animal Care and Use Committee.

### 2.2. Tissue collection

At two time points during drug administration (5 and 7 DPI) and at two time points following cessation of treatment (9 and 11 DPI), mice were euthanized by isoflurane overdose and perfused with 15 mL ice cold PBS following blood collection by cardiocentesis. Blood was allowed to coagulate in BD Microtainer serum separator tubes and centrifuged for 15 min at 1500 RCF. Serum was collected and stored at −20 °C. For RNA and plaque assay analysis, brains and spinal cords were collected, flash-frozen and stored at −80 °C. For histopathology and immunohistochemistry, mice were perfused with 40 mL cold 4% paraformaldehyde (PFA), and brains and spinal columns were collected. Brains were divided into three coronal sections using an Adult Mouse Brain Slicer (Zivic Instruments), fixed overnight in 4% PFA at 4 °C, and washed in ice-cold PBS. Spinal columns were trimmed of excess soft tissue, fixed overnight in 4% PFA at 4 °C, and then decalcified on a rotator for 24–36 h in a 10% sodium citrate/22% formic acid solution. Spinal columns were washed in ice-cold PBS and the L4-L6 regions were isolated. Tissues were embedded in paraffin for sectioning and staining.

### 2.3. Mononuclear cell isolation

Single cell suspensions were made from cervical lymph nodes (CLNs), brains, and spinal cords pooled from two to five mice per group per time point as previously described (Baxter and Griffin, 2016). Briefly, CLNs were dissociated using a gentleMACS Dissociator (Miltenyl Biotec), and red blood cells were lysed using ammonium chloride (Sigma-Aldrich). Brains and spinal cords were dissociated in RPMI containing collagenase and DNase in C tubes using a gentleMACS Dissociator. Mononuclear cells were separated from red blood cells and myelin debris on a 30%/70% Percoll gradient (GE Healthcare) for 30 min at 4 °C. Live mononuclear cells from all tissues were quantified by trypan blue exclusion.

### 2.4. Flow cytometry

Cells were stained and analyzed by flow cytometry as previously described (Baxter and Griffin, 2016). Briefly, $10^6$ live cells were stained with violet LIVE/DEAD Fixable Dead Cell Stain (Life Technologies) for 30 min, anti-mouse CD16/CD32 (BD Pharmingen) for 15 min, and monoclonal antibodies against CD45 (clone 30-F11), CD3 (clone 17A2), CD4 (clone RM4-5), CD8a (clone 53-6.7), and CD19 (clone 1D3) from Ebioscience or BD Pharmingen for 30 min. Cells were run on a BD FACSCanto II cytometer using BD FACSDiva software, version 8, and analyses were carried out using FlowJo software, version 8. Cells were characterized as follows: CD4 T cells ($CD45^{hi}CD3^+CD4^+$), CD8 T cells ($CD45^{hi}CD3^+CD8^+$), and B cells ($CD45^{hi}CD3^-CD19^+$). For CLN and brain, total mononuclear cell counts were from three independent experiments, and for spinal cord, as well as $CD4^+$, $CD8^+$ and $CD19^+$ cells for all tissues, counts were from two independent experiments. At 11 DPI, the SINV, 0.6 mg/kg DON group had data from one fewer experiment than the others (one to two independent experiments).

### 2.5. Histology and immunohistochemistry

Three to four 10 μm brain sections per mouse were stained with H & E, coded, and scored as previously described (Rowell and Griffin, 1999) using a 0–3 scale. A score of 0 was given when there was no detectable inflammation, a score of 1 for brains with one to two small inflammatory foci per section, a score of 2 for moderate inflammatory foci in up to 50% of 10X fields, and a score of 3 for moderate to large inflammatory foci in greater than 50% of 10X fields. An additional point was added for excessive parenchymal cellularity, allowing for a maximal score of 4.

Three to four 10 μm lumbar spinal cord sections per mouse were stained with H & E, coded, and scored using a 0–2 scale adapted from the brain scoring system. A score of 0 was given for no detectable inflammation, a score of 1 for one to two small inflammatory foci per section, and a score of 2 for greater than two inflammatory foci per spinal cord or for spinal cords with moderate to marked inflammatory foci. An additional point was added for excessive parenchymal cellularity, allowing for a maximal score of 3.

For immunohistochemical staining, 10 μm brain sections were deparaffinized and hydrated. Antigen retrieval was performed by boiling slides in 0.01 M sodium citrate, pH 6.0 (glial fibrillary acidic protein, GFAP), and endogenous peroxidase was quenched with 3% $H_2O_2$ in methanol for 10 min (ionized calcium binding adaptor molecule 1, IBA1 and glutamate transporter 1, GLT1). Slides were blocked in 10% normal goat serum (NGS), and incubated with primary antibody diluted in PBS +5% NGS +0.04% TritonX (GFAP 1:1000,

Millipore AB5804, 1 h RT; IBA1 1:200, Wako, 4 °C overnight; GLT1 1:100, [Rothstein et al., 1994], 4 °C overnight). Tissues being stained for GFAP were additionally treated with an Avidin/Biotin Blocking Kit (Vector Laboratories) prior to primary antibody incubation. Tissues were incubated in secondary anti-rabbit IgG (Vector Laboratories, 5 μg/mL in PBS +5% NGS +0.04% Triton X) for 1 h at RT with Vectastain Elite ABC kit (Vector Laboratories), and visualized with 3',3'-diaminobenzidine (DAB) peroxidase substrate (Vector). Tissues were counterstained with hematoxylin, dehydrated, and mounted with Permount (Fisher Scientific).

For TUNEL staining, 10 μm brain or spinal cord sections were rehydrated and treated with 1 mg/mL proteinase K (1:200 in deionized water) for 30 min for antigen retrieval. Endogenous peroxidases were quenched in methanol +3% $H_2O_2$ for 5 min, and after immersion in TdT Labeling Buffer for 5 min, sections were stained with TdT Labeling Reaction mix for 60 min at 37 °C in a humidity chamber. To stop the reaction, slides were immersed in TdT Stop Buffer for 5 min then incubated with streptavidin-HRP solution for 10 min (TACS 2 TdT kit, Trevigen). Tissues were developed with DAB for 8 min, counterstained with hematoxylin, dehydrated, and mounted with Permount. Slides were coded, and the whole visible hippocampus on one brain section per mouse or the entire spinal cord cross section was outlined to determine the tissue area using a Nikon Eclipse E600 microscope and StereoInvestigator software (MBF Bioscience). All TUNEL-positive cells, indicated by brown staining, were counted within the outlined area, and results were graphed as TUNEL-positive cells per $mm^2$ tissue.

For SINV antigen staining, 10 μm brain or spinal cord sections were rehydrated and treated with 1 mg/mL proteinase K (Invitrogen, 1:200) for 20 min for antigen retrieval. Endogenous peroxide was quenched in methanol +3% $H_2O_2$ for 10 min, and tissues were blocked with 10% NGS in PBS for 20 min. Slides were incubated with rabbit anti-sera to SINV (1:200 in PBS +5% NGS +0.04% Triton-X)(Jackson et al., 1988) for 60 min, biotinylated anti-rabbit IgG secondary antibody (5 μg/mL in PBS +5% NGS +0.04% Triton-X) for 30 min, and avidin-biotin complex (VECTASTAIN Elite ABC kit) for 40 min. Slides were developed with DAB, counterstained and mounted as above.

### 2.6. Immunoblotting

Protein was quantified in 20% w/v whole brain homogenates from two independent experiments with two individual mice per group in each experiment (total of four mice per group) using a DC assay kit (Bio Rad Laboratories). 10 μg samples were separated on a 10% SDS-PAGE gel and transferred to a nitrocellulose membrane (Bio Rad). After confirmation of protein presence using a 0.2% Ponceau S stain (Sigma Aldrich), membranes were blocked in 5% milk. Membranes were incubated overnight at 4 °C with anti-GFAP (1:50,000, Millipore), anti-IBA1 (1:1,000, Wako Chemical Laboratories), or anti-GLT1 (1:100,000; Rothstein et al., 1994) diluted in 5% BSA. Membranes were incubated with HRP-conjugated secondary anti-rabbit IgG (Cell Signaling) diluted in 5% milk (1:10,000, 1:2,000, and 1:50,000 for anti-GFAP, anti-IBA1, and anti-GLT1, respectively) for 1 h at RT. Membranes were developed using the Amersham ECL Prime Western Blot Developing kit (GE Healthcare). Membranes were then exposed either in a darkroom with Amersham Hyperfilm ECLHigher performance chemiluminescence film (GFAP, IBA1, and associated ACTB), or using a Bio-Rad Universal Hood II and ChemiDoc XRS imaging camera (GLT1 and associated ACTB). Densitometry measurements were performed using ImageJ Software, and the average fold-change of each protein normalized to ACTB compared to mock-infected, untreated control homogenates was calculated.

### 2.7. Protein quantification by enzyme immunoassay

Anti-SINV antibody was measured in serum and 20% w/v brain homogenates in three to four mice per group per time point using an in-house enzyme immunoassay (EIA) as previously described (Baxter and Griffin, 2016). Briefly, Maxisorp 96-well plates (Thermo Scientific Nunc) coated with PEG-purified SINV TE were blocked in PBS-0.05% Tween-20+10% FBS for 2 h at 37 °C and incubated overnight at 4 °C with samples (1:100 [IgM] or 1:10 [IgG] for serum, 1:4 for brain homogenates, diluted in PBS-0.05% Tween-20+10% FBS). After incubating wells with 1:1000 HRP-conjugated goat anti-mouse IgM or IgG (Southern Biotech) for 2 h at RT, plates were developed using a BD OptEIA TMB Substrate Reagent kit and stopped using 2 M $H_2SO_4$. Plates were read at 450 nm and the optical density (OD) values for infected mice minus the OD values for mock-infected mice were graphed.

Interferon-gamma (IFN-γ) production was quantified in 20% w/v brain homogenates in 3–5 mice per group per time point by commercial EIA kit (Ebioscience Ready-SET- Go!). Assays were performed according to manufacturer's instructions, and data are presented as pg per gram brain. The standard curve for the assay ranged from 312.5 to 20,000 pg/g.

### 2.8. Quantification of infectious virus

Ice-cold PBS was added to left halves of brains (20% w/v) or whole spinal cords (10% w/v) previously frozen and stored at −80 °C from 3 to 6 mice per group per time point. Tissues were homogenized in MP Biomedicals Lysing Matrix A tubes at 6.0 M/s for 40 s using a FastPrep-24 homogenizer (MP Biomedicals) and clarified by centrifuging at 13,200 rpm for 15 min at 4 °C. Supernatant fluids were serially diluted ten-fold in DMEM +1% FBS and incubated on BHK cells for 1 h, and an agarose overlay was applied. Assay plates were incubated at 37 °C, 5% $CO_2$ for 48 h, and plaques were counted using 10% neutral red solution to stain live cells and aid visualization. When a sample had no detectable plaques, a value of half the limit of detection for the assay was assigned.

### 2.9. qRT-PCR evaluation of IFN-γ mRNA expression and viral RNA production

Right brain halves and whole spinal cords from three to five mice per group per time point were placed in Lysing Matrix D tubes and homogenized in 1.0 mL Qiazol at 6.0 M/s for 40 s in a FastPrep-24 homogenizer (MP Biomedicals). RNA was isolated using the Qiagen RNeasy Lipid Mini kit and cDNA was synthesized with random primers using a Life Technologies High Capacity cDNA Reverse Transcription Kit. qRT-PCR was performed using TaqMan Universal PCR Master Mix (Roche) on a 7500 Fast Real-Time PCR System for 50 cycles, and results were analyzed using Sequence Detector software, version 1.4. *Ifng* mRNA was measured using a commercially available TaqMan gene expression assay (Integrated DNA Technologies), and relative gene expression versus mock-infected mice was determined by the ΔΔCT method using mouse *Gapdh* for normalization. SINV RNA copies were measured using TaqMan probe (5'–6-carboxyfluorescein [FAM]-CGCATACAGACTTCCGCCCAGT–6-carboxytetramethylrhodamine [TAMRA]–3' (Applied Biosystems) and primers to the SINV E2 gene (forward, 5'-TGGGACGAAGCGGACGATAA-3'; reverse, 5'-CTGCTCCGCTTTGGTCGTAT-3'). SINV E2 copies were quantified using a standard curve made of ten-fold dilutions of a plasmid containing the SINV subgenomic region and normalized to endogenous mouse *Gapdh*.

### 2.10. Statistics

Statistical analyses were performed using GraphPad Prism 6 software. Time-course studies were analyzed by two-way ANOVA with Tukey's multiple comparison post-test, and single time point studies were analyzed by one-way ANOVA with Tukey's multiple comparison post-test. A $p$ value of $< 0.05$ was considered significant in all analyses.

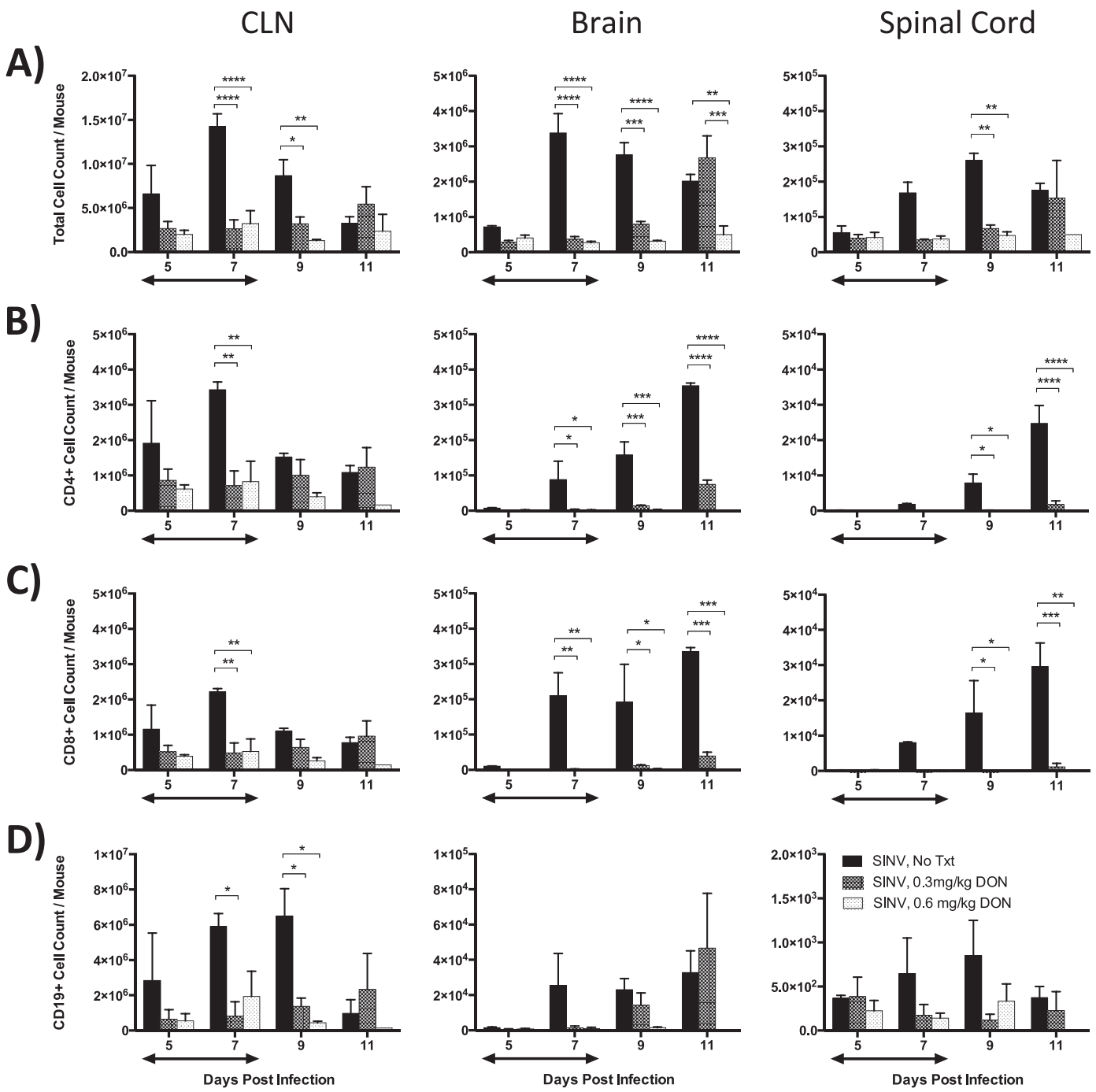


**Fig. 1.** Immune cell proliferation in the periphery and infiltration into the CNS in DON-treated, SINV-infected mice. Absolute numbers of total live mononuclear cells by trypan blue exclusion (**A**), $CD4^+$ T cells (**B**), $CD8^+$ T cells (**C**), and $CD19^+$ B cells (**D**) in the cervical lymph nodes (CLNs) (left panel), brains (middle panel), and spinal cords (right panel) of SINV-infected mice receiving no treatment (Txt), low (0.3 mg/kg) dose DON, or high (0.6 mg/kg) dose DON at 5, 7, 9, and 11 DPI (n =2–5 pooled mice per group per time point from 2 to 3 independent experiments, except for SINV, 0.6 mg/kg DON group at 11 DPI, which is from 1 to 2 independent experiments; data presented as the mean ± SEM; double-headed arrows indicate the period of DON treatment; $*p < 0.05$, $**p < 0.01$, $***p < 0.001$, $****p < 0.0001$, by Tukey's multiple comparisons test).

## 3. Results

### *3.1. Glutamine antagonism prevents lymphocyte proliferation in the draining cervical lymph nodes and mononuclear cell infiltration into the CNS*

To determine the effect of DON treatment beginning at the time of infection on induction of the immune response in the periphery and on entry of immune cells into the CNS, the draining cervical lymph nodes (CLNs) and CNS tissues were examined from mice infected intranasally with the TE strain of SINV. Because lymphocyte proliferation in response to antigen stimulation requires utilization of glutamine as an energy source (Maciolek et al., 2014), we hypothesized that treatment with DON would reduce production of SINV-specific lymphocytes and infiltration of immune cells into the CNS during SINV infection. To examine the effect of daily low (0.3 mg/kg) and high (0.6 mg/kg) doses of DON on the cellular immune response to infection, changes in the numbers of total cells and of $CD4^+$ and $CD8^+$ T cells and B cells were evaluated in the CLNs, brains, and spinal cords of SINV-infected mice during DON treatment (5 and 7 DPI) and after cessation of treatment (9 and 11 DPI) (Fig. 1). Mononuclear cells were isolated from tissue homogenates, total live cells were counted

(Fig. 1A), and numbers of $CD4^+$ T cells (Fig. 1B), $CD8^+$ T cells (Fig. 1C), and $CD19^+$ B cells (Fig. 1D) were determined by flow cytometry.

In the CLNs, all cell types increased in untreated, SINV-infected mice, with the highest numbers of total mononuclear cells, $CD4^+$ T cells and $CD8^+$ T cells at 7 DPI, and highest numbers of $CD19^+$ B cells at 9 DPI. In DON-treated, SINV-infected mice, CLN cell numbers did not begin to increase until 11 DPI in mice that had received DON at the low dose and did not increase during the period of observation for mice that received DON at the high dose.

In the brains and spinal cords of untreated, SINV-infected mice, total numbers of mononuclear cells increased starting at 7 DPI and peaked between 7 and 9 DPI. In both tissues, $CD4^+$, $CD8^+$, and $CD19^+$ cell populations steadily increased in number, peaking at 11 DPI. In DON-treated, SINV-infected mice, there was no evidence of infiltration of any cell population into the brain or spinal cord at days 5 or 7 during treatment. However, after cessation of treatment, total mononuclear cells and $CD19^+$ B cells increased at 9 DPI, and $CD4^+$ and $CD8^+$ T cells were evident in the brain at 11 DPI in mice treated with the low DON dose. Similar increases in infiltrating cells into the spinal cords of DON-treated mice were not seen during this time. Taken together, these data indicate that DON treatment inhibits proliferation of T and B cells in the periphery in response to SINV infection, resulting in decreased infiltration of immune cells into the CNS. With cessation of DON treatment the immune response was gradually activated.

### 3.2. Glutamine antagonism decreases CNS inflammation and pathology during SINV infection

To examine the effect of glutamine antagonism on CNS pathology during SINV infection, coronal brain sections (Fig. 2) and transverse lumbar spinal cord (Fig. 3) sections of SINV-infected mice untreated or treated with low or high dose DON were stained with H & E and evaluated for pathological changes and evidence of inflammation. While inflammation and pathological changes were present throughout the brain, the hippocampus was chosen for closer evaluation due to the predilection of SINV for those neurons (Kimura and Griffin, 2003). In the hippocampi and spinal cords of untreated, SINV-infected mice, perivascular cuffs of mononuclear cells and increased parenchymal cellularity were appreciable by 7 DPI (Figs. 2A and 3A). At 7 and 9 DPI, there was disruption of neuronal architecture in the hippocampus, with multifocal areas of granule cell loss and immune cell infiltration in the dentate gyrus (Fig. 2A), and at 9 DPI, tissue necrosis was noted in the lateral ventral horn of the spinal cord (Fig. 3A). Increased inflammation and pathological changes had resolved by 11 DPI. Compared to mock-infected controls (data not shown), there was no evidence of increased inflammation or pathological changes in the brains or spinal cords of SINV-infected mice treated with low or high dose DON during the period of drug administration. Following cessation of treatment, perivascular cuffs of mononuclear cells became apparent at 9 and 11 DPI in the hippocampi and spinal cords of SINV-infected mice previously treated with DON. Disruption of normal architecture in the granule layer of the dentate gyrus was noted at 11 DPI in SINV-infected mice previously treated with low dose DON.

To quantify the level of inflammation, H & E-stained slides were coded and scored (Rowell and Griffin, 1999). Brain inflammation scores significantly differed among groups (Fig. 2B; $p < 0.001$, two-way ANOVA), with untreated, SINV-infected mice having higher scores than SINV-infected, low dose DON-treated mice at 7 DPI, and SINV-infected, high dose DON-treated mice at 5, 7, and 9 DPI. Inflammation scores began to decrease at 11 DPI in untreated mice. Starting at 9 DPI, following cessation of DON treatment, brain inflammation scores in SINV-infected, low dose DON-treated mice began to increase, becoming significantly higher than those of SINV-infected, high dose DON-treated mice at 9 DPI and significantly higher than those of untreated, SINV-infected mice at 11 DPI. Inflammation scores in SINV-infected, high dose DON-treated mouse brains began to increase at 11 DPI.

Lumbar spinal cords scored for inflammation showed trends that were similar to brains (Fig. 3B). Inflammation scores differed significantly among groups ($p < 0.001$, two-way ANOVA), with scores in untreated, SINV-infected mice significantly higher than those of SINV-infected, low dose DON-treated mice at 7 DPI and significantly higher than those of SINV-infected, high dose DON-treated mice at 7 and 9 DPI. Following cessation of treatment, inflammation scores began to increase in SINV-infected, low dose DON-treated and SINV-infected, high dose DON-treated mice at 9 and 11 DPI, respectively. By 11 DPI, spinal cord inflammation scores were comparable among treatment groups. These data show that glutamine antagonism suppresses inflammation and CNS pathological changes due to SINV infection during treatment, but cessation of treatment results in appearance of inflammation over time in a dose-dependent manner.

### 3.3. Effect of treatment on brain markers associated with glutamate excitotoxicity

A mechanism that likely contributes to neuronal damage during alphavirus infection is glutamate excitotoxicity accompanied by glial cell activation (Darman et al., 2004; Greene et al., 2008; Nargi-Aizenman et al., 2004). To evaluate the potential role of DON treatment in mitigating glutamate excitotoxicity during SINV infection, glial cell markers associated with glutamate excitotoxicity during virus infection were examined (Brison et al., 2011; Darman et al., 2004). Expression of GFAP and GLT1 by astrocytes and IBA1 by microglial cells was assessed by immunohistochemistry (IHC) and immunoblot. To maximize the chance of observing an effect, markers were examined at 7 DPI during the period of DON treatment.

GFAP is an intermediate filament protein highly expressed by activated astrocytes (Eng and Ghirnikar, 1994). GFAP expression increased with SINV infection as assessed by both IHC and immunoblot (Figs. 4A, D). Overall levels of protein differed among groups (Fig. 4G; $p < 0.05$, one-way ANOVA) but were not affected by DON treatment, suggesting that the increase in GFAP is a direct result of the local innate response to neuronal virus infection (Carpentier et al., 2004).

GLT1, also known as EAAT2, is an astrocyte transporter protein responsible for most glutamate scavenging within the CNS (Danbolt, 2001). In control brains, GLT1 was highly expressed with widespread staining in the extraneuronal mileu. During SINV infection, GLT1 expression in the hippocampus was variable with areas devoid of IHC staining (Fig. 4B) and an overall decrease in expression on immunoblot (Fig. 4E). In DON-treated mice, GLT1 distribution by IHC was restored to that found in mock-infected, untreated control mice. GLT1 protein levels for individual mice on immunoblot were variable and density quantification did not identify significant differences between groups (Fig. 4H).

IBA1 is a cytoplasmic protein specifically expressed by macrophages and microglia and upregulated during cellular activation (Ito et al., 1998). During SINV infection, IBA1 expression was increased by both IHC and immunoblot compared to mock-infected, untreated controls (Figs. 4C, F and I; $p < 0.001$, one-way ANOVA). Compared to brains from SINV-infected, untreated mice, IBA1 was less highly expressed in brains from mice treated with DON, but was not reduced to control levels. For all three markers, DON treatment had no appreciable impact on protein expression in brains from mock-infected mice by IHC (data not shown). Therefore, DON treatment of SINV-infected mice had a variable effect on markers of glial cell activation associated with glutamate excitotoxicity.

### 3.4. DON treatment decreases apoptosis in the CNS during SINV infection

Death of neurons during viral infection results in significant organ dysfunction. To evaluate whether DON treatment decreases cell death in

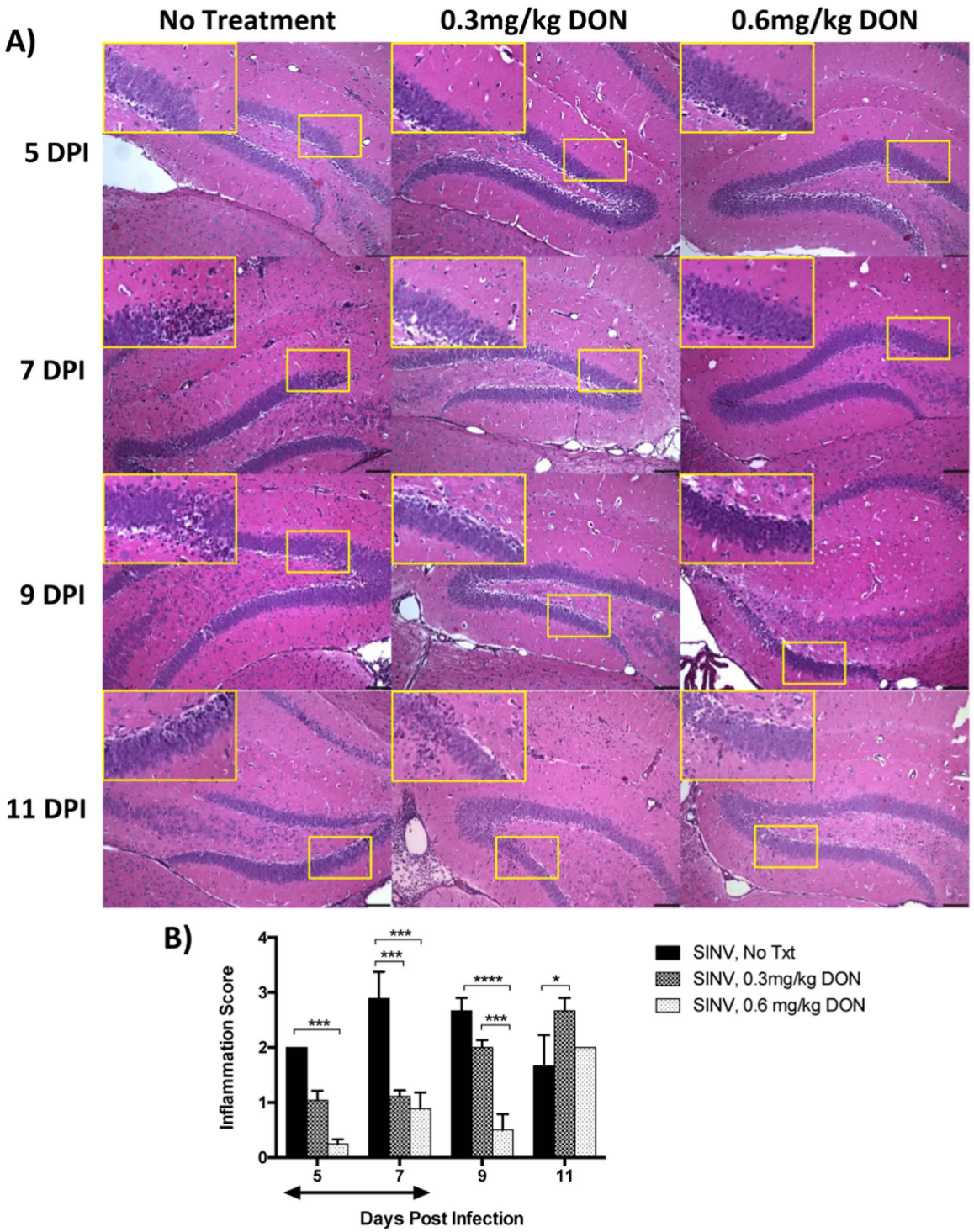


**Fig. 2.** Effect of DON treatment on pathology and brain inflammation during SINV infection. (**A**) Representative photomicrographs of H & E sections of the hippocampus of SINV-infected mice receiving no treatment, low (0.3 mg/kg) dose DON, or high (0.6 mg/kg) dose DON at 5, 7, 9, and 11 DPI. Insets show disruption of granular cell layer architecture of the dentate gyrus with loss of granule cells and infiltration of inflammatory cells (100X magnification; scale bar=100 μm). (**B**) H & E sections of hippocampi of SINV-infected mice receiving no treatment, low dose DON, or high dose DON were scored for inflammation at 5, 7, 9 and 11 DPI using a four-point system (n =3–4 mice per group per time point; data presented as the mean ± SEM; double-headed arrows indicate the period of DON treatment; $^{*}p < 0.05$, $^{***}p < 0.001$, $^{****}p < 0.0001$ by Tukey's multiple comparisons test).

the brain and spinal cord during SINV infection, coronal brain sections and transverse lumbar spinal cord sections from SINV-infected mice treated with low or high dose DON were examined by TUNEL staining. Increased numbers of TUNEL-positive cells were present at 7 and 9 DPI in the hippocampi of SINV-infected mice (Fig. 5A). TUNEL-positive cells were only rarely detectable in hippocampi of SINV-infected mice treated with low or high dose DON during the period of treatment, but increased in frequency within the granular cell layer of the dentate gyrus at 9 DPI. At 11 DPI, TUNEL-positive cells were only rarely found in the hippocampi of all groups. In spinal cord sections of SINV-infected mice TUNEL-positive cells were present throughout at 7 and 9 DPI with fewer at either 5 or 11 DPI (Fig. 6A). TUNEL-positive cells were only rarely present in spinal cords of SINV-infected mice treated with low or high dose DON at any of the time points.

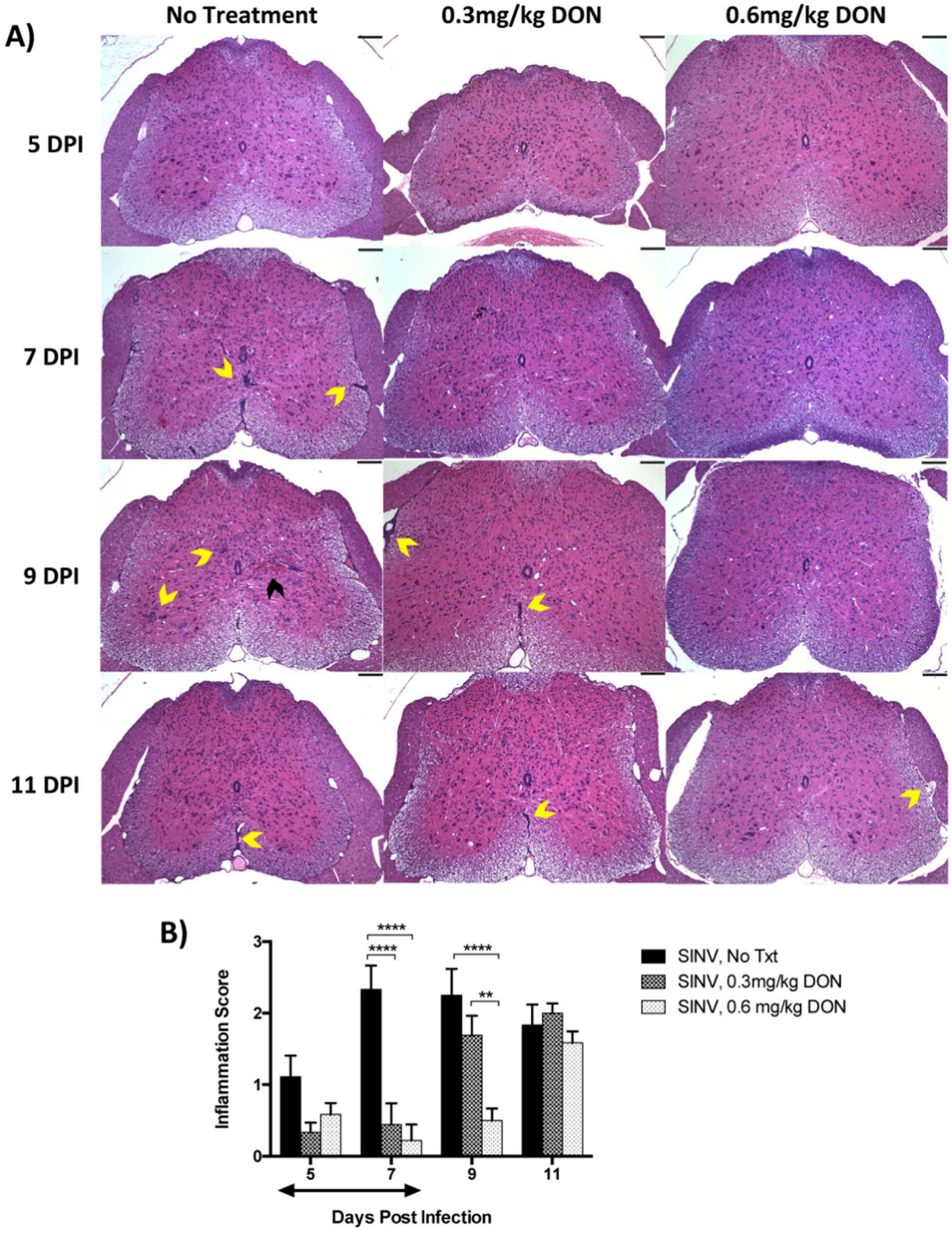


**Fig. 3.** Effect of DON treatment on spinal cord inflammation and pathology during SINV infection. (**A**) Representative photomicrographs of H & E sections of the spinal cords of SINV-infected mice receiving no treatment, low (0.3 mg/kg) dose DON, or high (0.6 mg/kg) dose DON at 5, 7, 9, and 11 DPI. Yellow arrowheads denote perivascular cuffs of mononuclear cells and infiltration of inflammatory cells into the parenchyma, and black arrowheads denote areas where normal tissue architecture has been disrupted (100X magnification; scale bar=100 μm). (**B**) H & E sections of spinal cords of SINV-infected mice receiving no treatment (Txt), low (0.3 mg/kg) dose DON, or high (0.6 mg/kg) dose DON were scored for inflammation at 5, 7, 9 and 11 DPI using a three-point system (n =3–4 mice per group per time point; data presented as the mean ± SEM; double-headed arrows indicate the period of DON treatment; $^{**}p < 0.01$, $^{****}p < 0.0001$ by Tukey's multiple comparisons test).

Quantification of TUNEL-positive cells showed that untreated, SINV-infected mice had more cell death than SINV-infected, low or high dose DON-treated mice in the hippocampus at 9 DPI (Fig. 5B) and in the spinal cord at 7 and 9 DPI (Fig. 6B). Evidence of cell death was comparable between groups at 5 and 11 DPI in both tissues.

### *3.5. Glutamine antagonism suppresses the antiviral immune response during SINV infection*

Previous studies have shown that clearance of infectious SINV from the CNS is affected synergistically by B cell-produced antibody directed

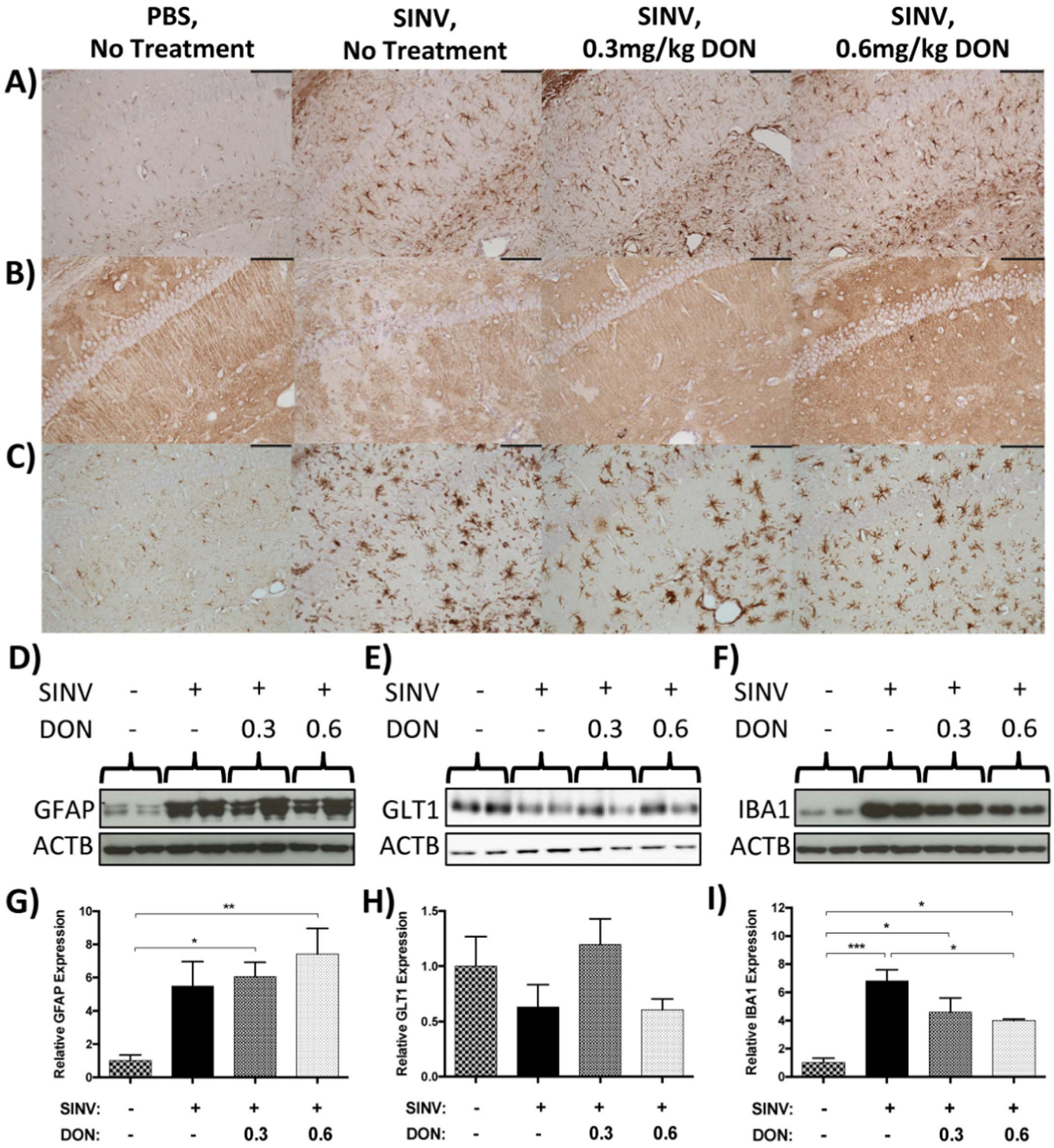


**Fig. 4.** Effect of DON treatment on brain expression of markers of glutamate excitotoxicity 7 days after SINV infection. **(A-C)** Representative photomicrographs of the CA1 region of hippocampus sections stained for GFAP (**A**), GLT1 (**B**), and IBA1 (**C**) of mock-infected or SINV-infected mice receiving no treatment, low (0.3 mg/kg) dose DON, or high (0.6 mg/kg) dose DON at 7 DPI (n =3 mice per group; brown staining = positive antigen; 200X magnification; scale bar=100 μm). (**D-I**) GFAP (**D**), GLT1 (**E**), and IBA1 (**F**) expression was examined by immunoblot in whole brains of mock-infected or SINV-infected mice receiving no treatment, low (0.3 mg/kg) dose DON, or high (0.6 mg/kg) dose DON at 7 DPI. Relative whole brain expression of ACTB-normalized GFAP (**G**), GLT1 (**H**), and IBA1 (**I**) was quantified and compared to mock-infected control brains (n =4 mice per group combined from 2 independent experiments; data presented as the mean ± SEM; $^{*}p < 0.05$, $^{**}p < 0.01$, $^{***}p < 0.001$, by Tukey's multiple comparisons test).

against the SINV E2 glycoprotein and T cell-produced IFN-γ (Binder and Griffin, 2001; Levine et al., 1991). Because glutamine antagonism suppresses lymphocyte proliferation (Colombo et al., 2010; Newsholme et al., 1985; Wang et al., 2011) (Fig. 1), the antiviral effector function of these cells was evaluated during and following DON treatment of SINV infection. Levels of SINV-specific IgM and IgG were evaluated in the sera and brains of SINV-infected, DON-treated mice by EIA (Fig. 7A-D). Serum IgM (Fig. 7A) and IgG (Fig. 7B) were both significantly higher in untreated mice compared to low and high dose DON-treated mice ($p < 0.01$ for IgM, $p < 0.0001$ for IgG, two-way ANOVA) at all time

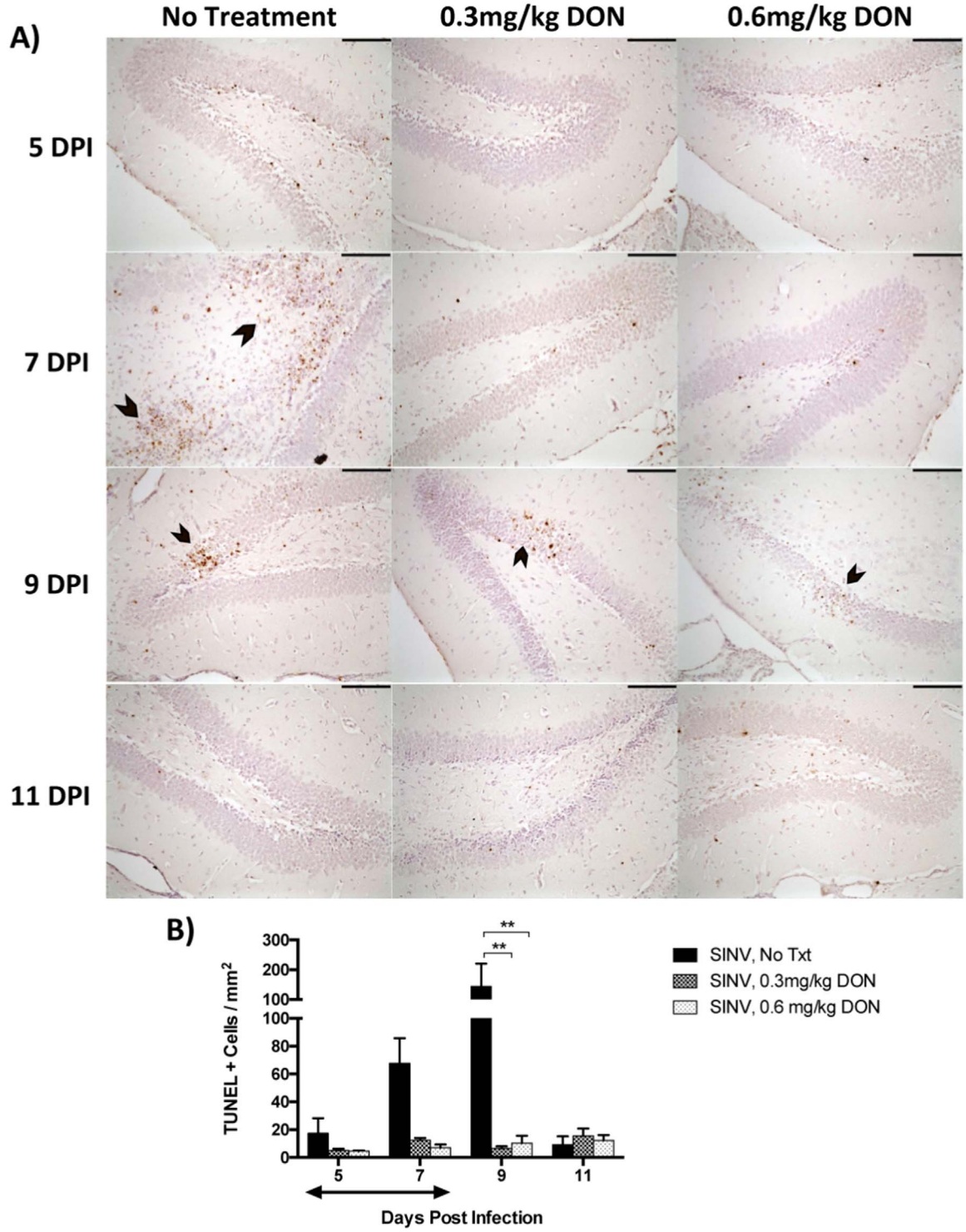


**Fig. 5.** Effect of DON-treatment on cell death in the hippocampus during SINV infection. (**A**) Representative photomicrographs of TUNEL staining in the dentate gyrus in the hippocampus of SINV-infected mice receiving no treatment, low (0.3 mg/kg) dose DON or high (0.6 mg/kg) dose DON at 5, 7, 9, and 11 DPI (brown nuclear staining=TUNEL-positive [denoted by black arrowheads]; 200X magnification; scale bar=100 μm). (**B**) Quantification of TUNEL-positive cells in hippocampi of SINV-infected mice receiving no treatment, low dose DON, or high dose DON at 5, 7, 9 and 11 DPI (n =3–4 mice per group per time point; data presented as the mean ± SEM; double-headed arrows indicate the period of DON treatment; $^{**}p < 0.01$, by Tukey's multiple comparisons test).

points for IgM and at 7, 9, and 11 DPI for IgG. Anti-SINV IgM and IgG in the sera of low and high dose DON-treated mice increased following cessation of treatment at 11 DPI.

SINV-specific brain IgM (Fig. 7C) and IgG (Fig. 7D) differed among treatment groups ($p < 0.0001$ for both IgM and IgG, two-way ANOVA) but increases were delayed in comparison to appearance of antibody in serum. Brain anti-SINV antibody was higher in untreated mice compared to both low and high dose DON-treated mice at 11 DPI for IgM and at 9 and 11 DPI for IgG. Anti-SINV IgM and IgG increased in the brains of low dose DON-treated, but not high dose DON-treated mice following cessation of treatment. These results show that glutamine antagonism decreases anti-SINV antibody production in the serum and brain during SINV infection, and that cessation of treatment allows increases in production.

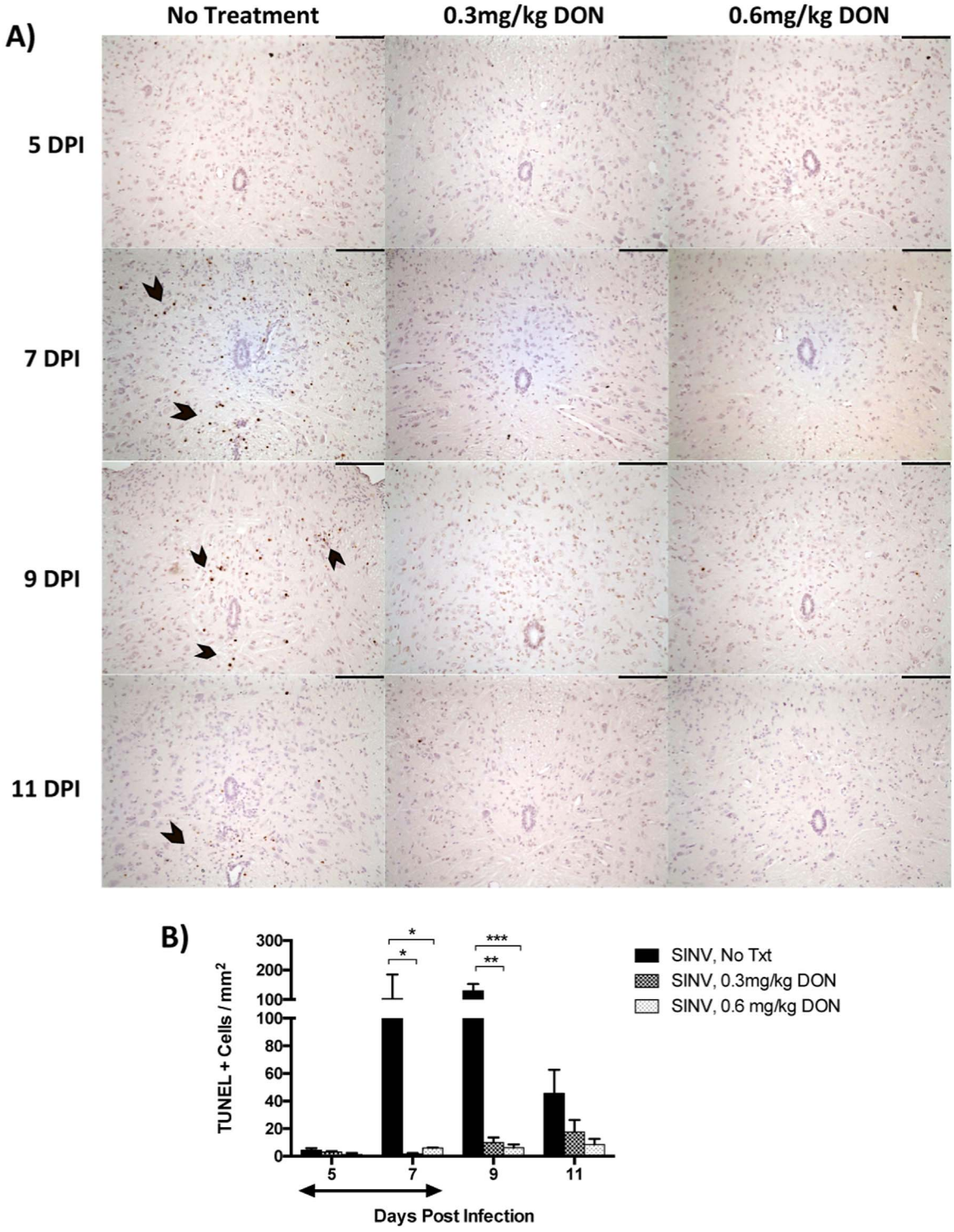


**Fig. 6.** Effect of DON-treatment on cell death in the spinal cord during SINV infection. (**A**) Representative photomicrographs of TUNEL staining of the gray matter in the spinal cord of SINV-infected mice receiving no treatment, low (0.3 mg/kg) dose DON or high (0.6 mg/kg) dose DON at 5, 7, 9, and 11 DPI (brown nuclear staining=TUNEL-positive [denoted by black arrowheads]; 200X magnification; scale bar=100 μm). (**B**) Quantification of TUNEL-positive cells in spinal cords of SINV-infected mice receiving no treatment, low (0.3 mg/kg) dose DON, or high (0.6 mg/kg) dose DON at 5, 7, 9 and 11 DPI (n =3–4 mice per group per time point; data presented as the mean ± SEM; double-headed arrows indicate the period of DON treatment; $^{*}p < 0.05$, $^{**}p < 0.01$, $^{***}p < 0.001$, by Tukey's multiple comparisons test).

IFN-γ also contributes to virus clearance (Binder and Griffin, 2001), and the effect of glutamine antagonism on expression in the brain during SINV infection of the CNS was examined by measuring levels of *Ifng* mRNA by qRT-PCR and levels of IFN-γ protein by EIA. Overall *Ifng* mRNA expression, when normalized to that of untreated, mock-infected mouse brain, significantly differed among groups (Fig. 7E; $p <$ 0.001, two-way ANOVA), with untreated, SINV-infected mice having increased expression at 7 DPI compared to low and high dose DON-treated mice. *Ifng* mRNA expression in brains of SINV-infected, low and high dose DON-treated mice was approximately 100-1000-fold higher than untreated-mock-infected mice. Following cessation of DON treatment, *Ifng* expression increased starting at 9 DPI, with SINV-

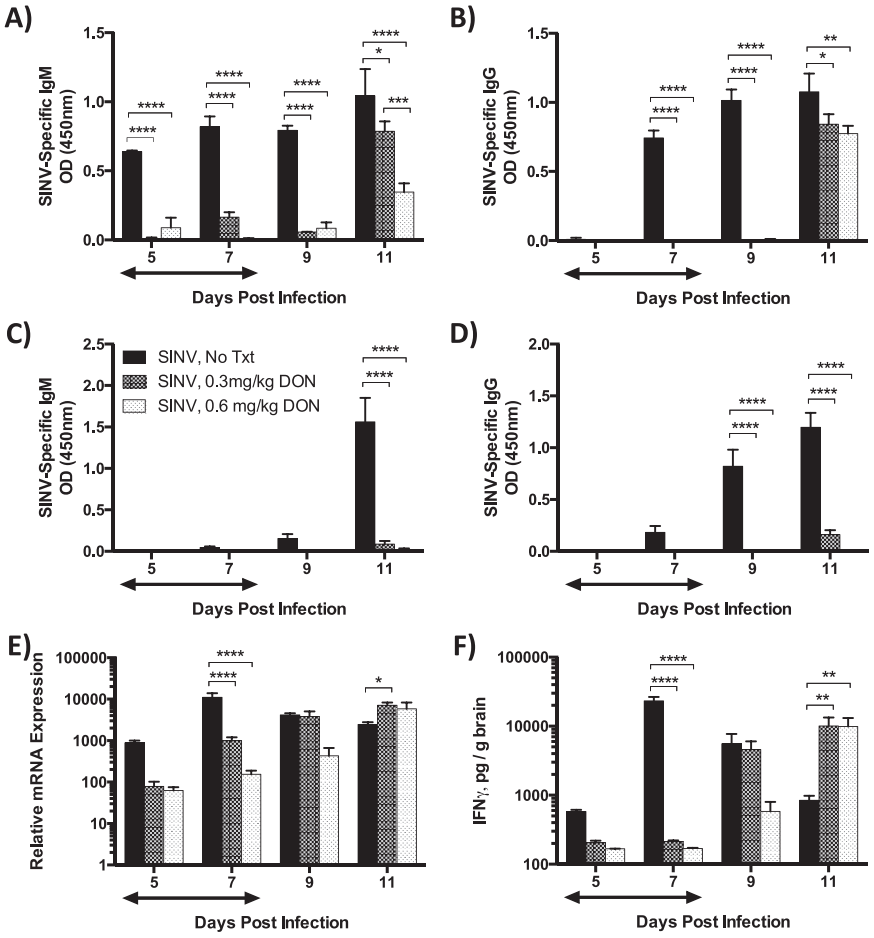


**Fig. 7.** Effect of DON treatment on SINV-specific antibody and IFN-γ production. (**A-D**) SINV-specific IgM (**A, C**) and IgG (**B, D**) levels were measured by ELISA in the serum (**A, B**) and brain (**C, D**) of SINV-infected mice receiving no treatment, low (0.3 mg/kg) dose DON, or high (0.6 mg/kg) dose DON at 5, 7, 9 and 11 DPI. (**E, F**) *Ifng* mRNA expression (**E**) was measured by RT-qPCR and IFN-γ protein levels (**F**) were measured by ELISA in the brains of SINV-infected mice receiving no treatment, low (0.3 mg/kg) dose DON, or high (0.6 mg/kg) dose DON at 5, 7, 9 and 11 DPI (n =3–5 mice per group per time point; data presented as the mean ± SEM; double-headed arrows indicate the period of DON treatment; *$p < 0.05$, **$p < 0.01$, ***$p < 0.001$, ****$p < 0.0001$ by Tukey's multiple comparisons test).

infected, low dose DON-treated mice having increased expression compared to untreated, SINV-infected mice at 11 DPI. *Ifng* expression in mock-infected, high dose DON-treated mouse brains was comparable to that of untreated, mock-infected mouse brains (data not shown).

IFN-γ protein levels in the brain significantly differed among groups (Fig. 7F; $p < 0.0001$, two-way ANOVA), with untreated, SINV-infected mice having higher expression at 7 DPI compared to low and high dose DON-treated mice. Following cessation of DON treatment, IFN-γ expression increased starting at 9 DPI, with both SINV-infected, low and high dose DON-treated mice having significantly increased expression compared to untreated, SINV-infected mice at 11 DPI. IFN-γ levels were below the level of detection in the brains of mock-infected mice and in brains of SINV-infected, low and high dose DON-treated mice during the period of drug administration at 5 and 7 DPI. These data show that glutamine antagonism impairs the two major adaptive antiviral responses involved in clearance of SINV.

### *3.6. DON treatment delays virus clearance in the brain and spinal cord*

Because the two major mechanisms by which the immune response clears SINV from the CNS were affected by glutamine antagonism, virus production was examined. SINV protein visualized in coronal brain (Fig. 8) and lumbar spinal cord (Fig. 9) sections by IHC showed the presence of SINV antigen in the hippocampus of untreated mice at 5, 7, and 9 DPI (Fig. 8A) and in the spinal cord at 7 and 9 DPI (Fig. 9A). Comparable levels of SINV antigen staining were found in mice treated with low or high dose DON in both tissues. Additionally, SINV antigen was readily visualized in the brains and spinal cords of DON-treated, but not untreated, mice at 11 DPI, although following cessation of DON administration, SINV protein began to decrease in DON-treated mice. DON treatment did not affect the distribution of SINV antigen in the brain or spinal cord.

Clearance of infectious virus was evaluated by measuring virus titers by plaque assay. Clearance from the brain was delayed in DON-treated mice in a dose-dependent manner, with titers significantly higher in DON-treated mice at 9 and 11 DPI (Fig. 8B). Virus titers were also significantly higher in spinal cords of DON-treated mice compared to untreated mice at 7, 9, and 11 DPI (Fig. 9B).

Viral RNA clearance was evaluated by measuring viral RNA levels by qRT-PCR. Clearance was delayed in DON-treated mice, with RNA copies significantly higher than untreated mice at 7, 9, and 11 DPI in the brain (Fig. 8C) and at 9 and 11 DPI in the spinal cord (Fig. 9C). Viral RNA levels began to decrease in brains of DON-treated mice following cessation of drug administration, although not to the same degree as infectious virus. Therefore, in addition to suppressing the immune response during SINV infection, glutamine antagonism delays virus clearance from the CNS.

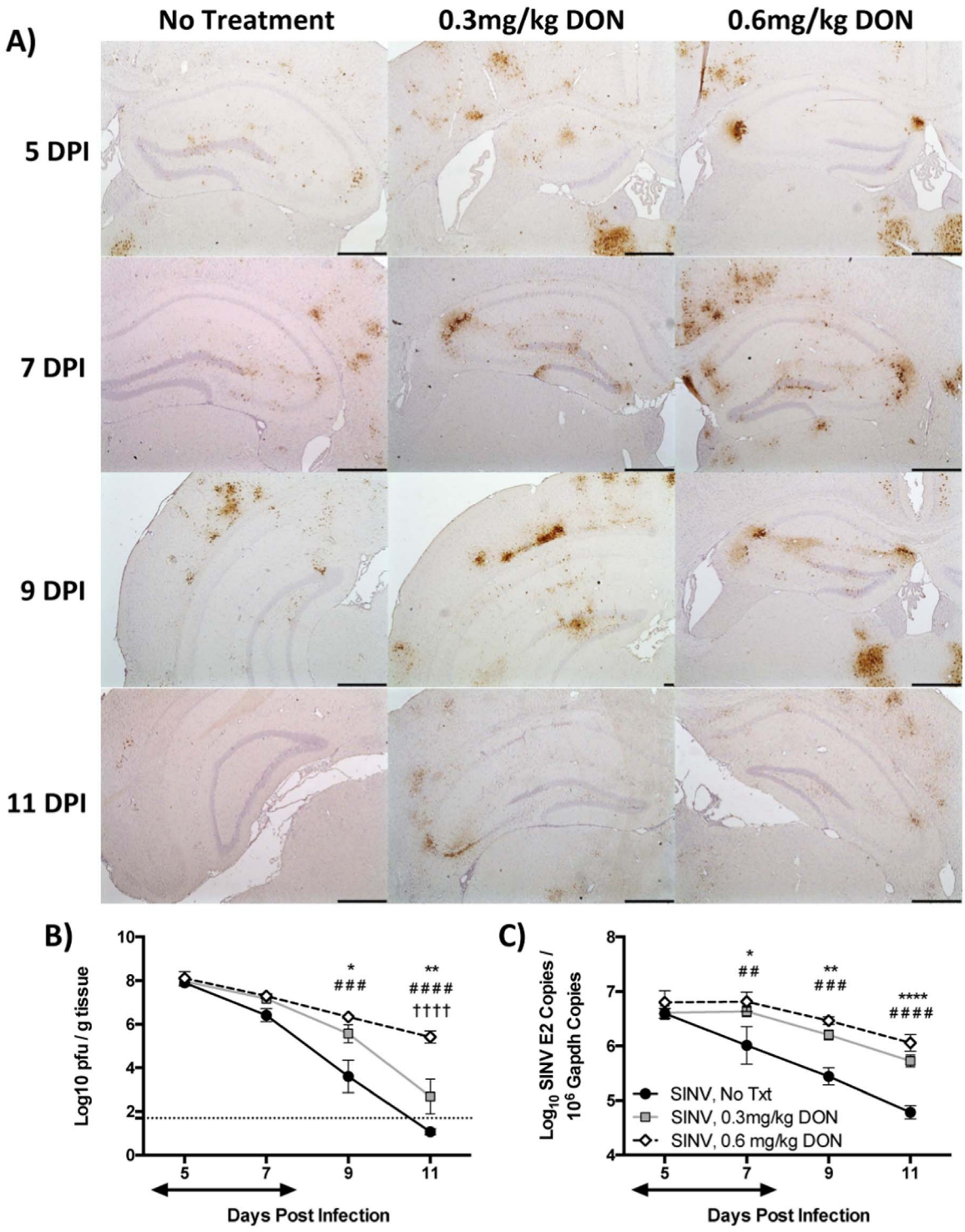


**Fig. 8.** Effect of DON treatment on SINV production and clearance in the brain. (**A**) Representative photomicrographs of immunohistochemical staining for SINV antigen in the hippocampus of SINV-infected mice receiving no treatment, low (0.3 mg/kg) dose DON, or high (0.6 mg/kg) dose DON in the brain at 5, 7, 9, and 11 DPI (SINV antigen = brown staining; 40X magnification, scale bar=500 μm). (**B**) Infectious virus titers were measured by plaque assay in the brains of SINV-infected mice receiving no treatment (black circle and line), low dose DON (gray square and line), and high dose DON (white diamond and black line). (**C**) Viral RNA levels were measured by qRT-PCR in the brains of SINV-infected mice receiving no treatment, low dose DON, and high dose DON (n =3–6 mice per group per time point; data presented as the mean ± SEM; double-headed arrows indicate the period of DON treatment; dotted line indicates assay limit of detection; $^{*}p < 0.05$, $^{**}p < 0.01$, $^{****}p < 0.0001$, untreated vs low dose DON; $^{\#\#}p < 0.01$, $^{\#\#\#}p < 0.001$, $^{\#\#\#\#}p < 0.0001$, untreated vs high dose DON; $^{\dagger\dagger\dagger\dagger}p < 0.0001$, low dose DON vs high dose DON, all by Tukey's multiple comparisons test).

## 4. Discussion

In this study, we sought to determine the mechanisms by which glutamine antagonism protects mice from neurologic deficits during nonfatal alphavirus encephalomyelitis. Treatment with DON for one week after infection impaired proliferation of lymphocytes in the draining CLNs and infiltration of mononuclear cells into the brain and spinal cord. This impaired immune response resulted in a decrease in pathological changes and fewer TUNEL- positive cells in the CNS but also reduced production of SINV-specific antibody and IFN-γ, resulting

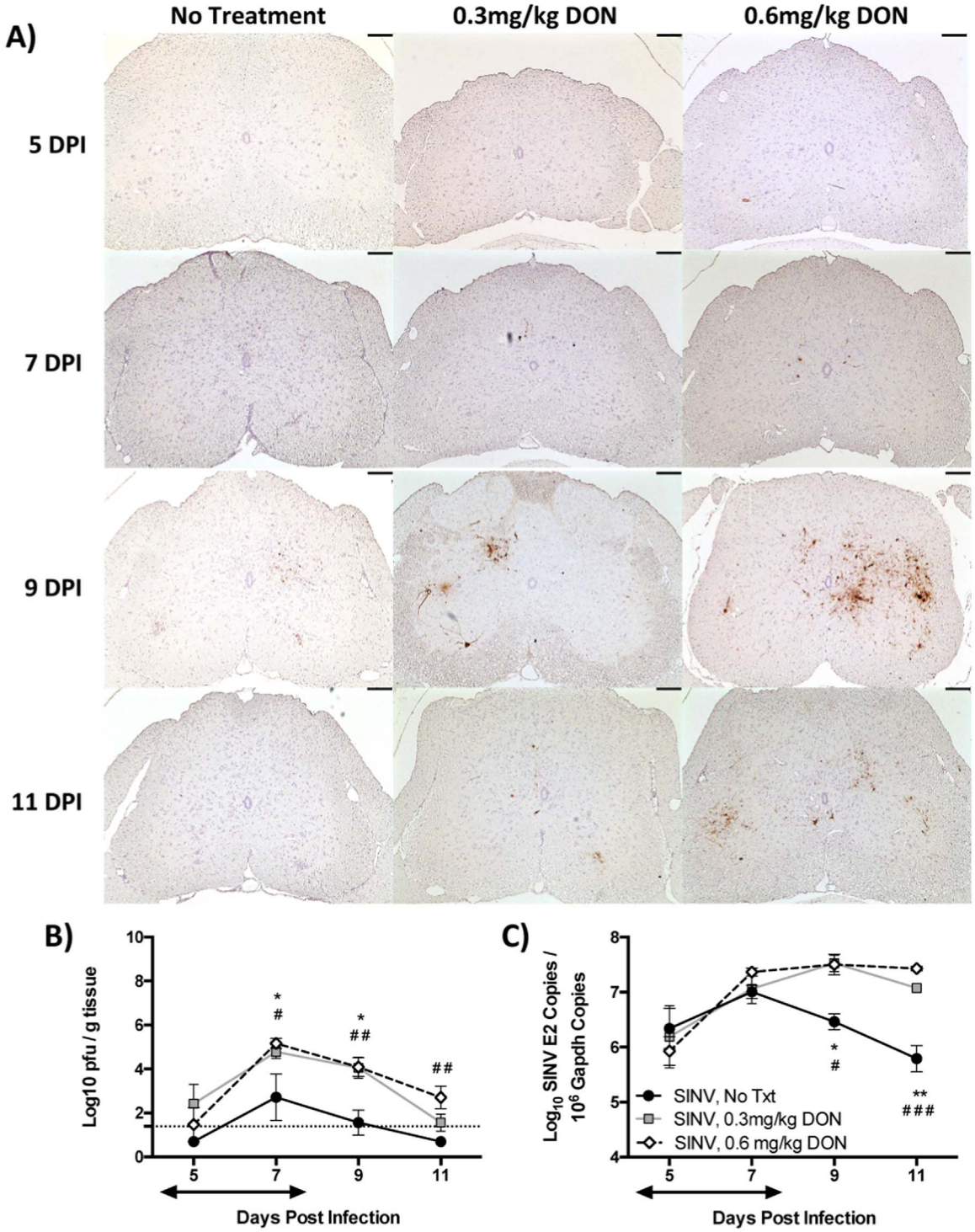


**Fig. 9.** Effect of DON treatment on SINV production and clearance in the spinal cord. (**A**) Representative photomicrographs of immunohistochemical staining for SINV antigen in SINV-infected mice receiving no treatment, low (0.3 mg/kg) dose DON, or high (0.6 mg/kg) dose DON in the spinal cord at 5, 7, 9, and 11 DPI (SINV antigen = brown staining; 100X magnification, scale bar=100 μm). (**B**) Infectious virus titers were measured by plaque assay in spinal cords of SINV-infected mice receiving no treatment, low dose DON, and high dose DON. (**C**) Viral RNA levels were measured by qRT-PCR in spinal cords of SINV-infected mice receiving no treatment (black circle and line), low dose DON (gray square and line), and high dose DON (white diamond and black line) (n =3–5 mice per group per time point; data presented as the mean ± SEM; double-headed arrows indicate the period of DON treatment; dotted line indicates assay limit of detection; $^{*}p < 0.05$, $^{**}p < 0.01$, untreated vs low dose DON; $^{\#}p < 0.05$, $^{\#\#}p < 0.01$, $^{\#\#\#}p < 0.001$, untreated vs high dose DON, all by Tukey's multiple comparisons test).

in delayed virus clearance. DON affected the immune response mostly during the period of treatment, so the effects on CNS pathology and virus clearance were transient and, upon cessation of treatment, the immune response was activated, CNS pathology appeared, and virus clearance initiated more quickly in low dose-treated than high dose-treated animals. DON had a variable effect on SINV-induced glial markers of glutamate excitotoxicity, suggesting that the primary mechanism for decreasing pathology is through modulation of the immune response.

When neurons are infected with a virus, three possible outcomes may occur (Griffin, 2011). First, the virus may directly kill the neuron by inducing processes such as apoptosis or necrosis (Havert et al.,

2000; Lewis et al., 1999, 1996). Second, the neuron may be damaged or die through a secondary process, such as effects of inflammation or glutamate excitotoxicity (Conrady et al., 2010; Greene et al., 2008). Activation of nearby microglia and astrocytes that release reactive oxygen and nitrogen species and infiltration of monocytes, neutrophils, and lymphocytes that release cytokines may all facilitate neuronal damage (Tilleux and Hermans, 2007). And lastly, virus infection of the neuron may be controlled through noncytolytic immune mechanisms so the cell survives. Because SINV RNA persists after infectious virus is cleared, the immune system must continually control virus reactivation.

Previous work has shown that in fatal alphavirus encephalomyelitis, neuronal death is primarily mediated through the immune response rather than direct viral mechanisms (Greene et al., 2008; Kimura and Griffin, 2003), and treatment with DON suppresses inflammation and reduces mortality (Manivannan et al., 2016). Likewise, in nonfatal SINV-induced encephalomyelitis, DON treatment reduces neurologic sequelae (Potter et al., 2015). However, neither of these studies included an in-depth examination of the effects of treatment on development of the immune response or on pathologic changes in the CNS during and after treatment.

This study shows that neurologic damage, including the more limited neuronal death, during nonfatal encephalomyelitis is immune-mediated rather than a direct effect of virus replication. Without treatment, mononuclear cells begin infiltrating the brain in high numbers by 7 DPI and TUNEL-positive cells peak after this, around 9 DPI. This is in contrast to peak infectious virus titers, which occurred at 5 DPI (and possibly earlier) in the brain. Despite having high virus titers throughout the time course, DON-treated mice had few TUNEL-positive cells in the hippocampus, corresponding with limited immune cell infiltration.

The immune system is the primary mediator of neuronal damage during fatal alphavirus encephalomyelitis. When mice lacking various components of cellular immunity are infected with NSV, mortality significantly decreases, indicating an important role for T cells (Rowell and Griffin, 2002). Furthermore, NSV-induced clinical disease development and mortality coincide with infiltration of $CD4^+$ and $CD8^+$ T cells into the brain (Kulcsar et al., 2014). In our study, neuronal loss and necrosis in the hippocampus and lumbar spinal cord corresponded with peak inflammation. During the period of DON treatment, mouse brains had fewer pathologic changes and fewer TUNEL-positive cells, previously shown to be neurons, compared to SINV-infected, untreated mice (Potter et al., 2015).

Due to the limited ability of neurons to regenerate, clearance of viruses that infect them requires a noncytolytic process to avoid long-term neurological deficits (Griffin, 2003). While innate production of type I IFN, particularly IFN-β, can help with the early control of SINV replication and spread, the adaptive immune response is responsible for virus clearance (Burdeinick-Kerr et al., 2007; Byrnes et al., 2000). SINV clearance from the CNS is achieved by a synergistic cooperation between SINV-specific antibody and IFN-γ (Baxter and Griffin, 2016; Burdeinick-Kerr et al., 2007).

By impairing proliferation of both B cells, which produce antibody, and T cells, which produce IFN-γ, virus clearance from both the brain and the spinal cord was delayed during the period of DON treatment. However, once treatment was stopped, levels of SINV-specific IgM and IgG increased in the serum, and IFN-γ mRNA expression and protein production increased in the brain. SINV-specific IgM and IgG were only detected in low dose DON-treated mouse brains at 11 DPI, while IgM was detectable in the serum of both low and high dose DON-treated mice at 9 DPI and at high levels at 11 DPI, further supporting the hypothesis that DON's primary effect on the immune system occurs in the periphery rather than the CNS in this mouse model.

Changes in brain IFN-γ levels in the different treatment groups over time closely followed that of mononuclear cell numbers (Fig. 1A) and H & E inflammation scores (Fig. 2B), but peak levels preceded peak infiltration of $CD4^+$ and $CD8^+$ T cells by two to four days (Figs. 1B and C) and quickly appeared after DON treatment was stopped. While macrophages can sometimes be a source of IFN-γ (Darwich et al., 2009), natural killer (NK) cells are more likely to be the non-T cell source of IFN-γ in this situation (Trinchieri et al., 1984). NK cells can be quickly activated to produce IFN-γ (Sun and Lanier, 2011) and proliferate in response to virus infection (Biron et al., 1983; Dokun et al., 2001; Sun et al., 2009; Lopez-Verges et al., 2011). However, the metabolic requirements for NK cell proliferation have not been extensively studied (Gardiner and Finlay, 2017), so the requirement for glutamine may be less than that of T cells. Therefore, we speculate that NK cells account for the early increase in *Ifng* mRNA and IFN-γ protein in the brains of DON-treated mice and contribute to the increases in untreated infected mice (Figs. 7E and F), but more investigation into this question is required.

Another secondary consequence of virus infection that contributes to neuronal damage and death is glutamate excitotoxicity. Glutamate is a major excitatory neurotransmitter that binds to glutamate receptors on recipient neurons (Sattler and Tymianski, 2001) and can result in an influx of excess calcium into the post-synaptic neuron, which in turn triggers a cascade resulting in free radical production and mitochondrial dysfunction, and ultimately, cell death (J. M. Lee et al., 1999; Nicotera and Orrenius, 1998). Hippocampal neurons in the brain and motor neurons in the spinal cord are especially sensitive to glutamate excitotoxicity (Carriedo et al., 2000; Nadler et al., 1978; Olney et al., 1979; Rothstein et al., 1993), and the process plays a role in SINV-induced pathology (Darman et al., 2004; Nargi-Aizenman et al., 2004). Furthermore, treatment with an AMPA receptor antagonist protects mice from NSV-induced death (Nargi-Aizenman et al., 2004; Greene et al., 2008).

To examine the effect of DON treatment on glutamate excitotoxicity, we examined the expression of several indirect markers of excitotoxicity. Expression of GFAP, an astrocyte protein up-regulated in response to neuronal damage and local cytokine production, was not affected by DON treatment, consistent with induction of an innate response to SINV infection. GLT1/EAAT2, which is primarily expressed by astrocytes but also found on microglia, is responsible for the majority of glutamate uptake from the synaptic cleft and thus an important player in the prevention of excitotoxicity (Danbolt, 2001). Several CNS virus infections, including NSV, human coronavirus (HCoV)-OC43, human T-lymphotropic virus, and human cytomegalovirus, downregulate GLT1 expression (Akaoka et al., 2001; Brison et al., 2011; Darman et al., 2004; Prow and Irani, 2008, 2007; Zhang et al., 2014), but others, including herpes simplex virus and Japanese encephalitis virus infection, induce upregulation (Mishra et al., 2007, 2008; Persson et al., 2007). In our study, SINV infection reduced GLT1 expression in the brain as determined by both IHC and immunoblot at 7 DPI compared to mock-infected control mice. However, DON treatment inconsistently restored expression of GLT1 in the brain at 7 DPI, with comparable expression of GFAP compared to untreated, SINV-infected mice.

Microglia are also a source of glutamate (Takeuchi and Suzumura, 2014), and microglial activation contributes to excitotoxicity during infection with several viruses, including HCoV, HIV, SIV, and Borna disease virus (Brison et al., 2011; Jiang et al., 2001; Koutsilieri et al., 1999; Ovanesov et al., 2007). Expression of IBA1, a marker of activated microglia, was increased in untreated, SINV-infected mouse brains compared to uninfected controls, and DON treatment decreased IBA1 expression at 7 DPI. However, macrophages also express IBA1 and infiltrate the brain during NSV infection (Kulcsar et al., 2014, 2015), so these cells could also be contributing to increased IBA1 expression during SINV infection. Further studies that directly measure glutamate and evaluate excitotoxicity, which are difficult to perform in vivo, would help elucidate the role glutamine antagonists play in preventing excitotoxicity.

The inability of DON to effectively cross the blood brain barrier

(BBB) could explain the inconsistent effect of drug administration on glutamate excitotoxicity (Alt et al., 2015; Potter et al., 2015). During SINV infection, approximately 50% of mice treated with DON develop clinical signs of encephalomyelitis by 7 DPI, compared to almost 100% of untreated, SINV-infected mice (Potter et al., 2015). Because the immune response is almost completely absent in CNS during the period of DON treatment, this suggests another mechanism, such as glutamate excitotoxicity, is contributing to clinical disease development. Therefore, while we can conclude that DON treatment suppresses immune cell proliferation in the periphery, leading to decreased cell death but delayed virus clearance in the CNS, it likely has less of an effect on glutamate excitotoxicity due to its poor ability to cross the BBB, resulting in residual clinical disease development. However, a prodrug version of DON containing a methyl-POM on the amine and isopropyl ester on the carboxylate that achieves a ten-fold higher cerebrospinal fluid to plasma ratio compared to the parent DON in rhesus macaques has been recently developed (Rais et al., 2016).

Treatment for alphavirus encephalomyelitis is currently limited to supportive care that is usually only initiated once clinical disease develops, and glutamine antagonists such as DON provide an attractive potential therapy. DON is effective against several tumors (Magill et al., 1957; Rais et al., 2016; Shelton et al., 2010; Sullivan et al., 1988), and its immune suppressive properties prevent allograft rejection and attenuate clinical signs associated with experimental autoimmune encephalomyelitis and *Plasmodium* infection (Gordon et al., 2015; Lee et al., 2015; Plaimas et al., 2013; Shijie et al., 2009). However, gastrointestinal toxicity observed both in mice (Potter et al., 2015; Rais et al., 2016) and in human trials (Earhart et al., 1990, 1982; Sklaroff et al., 1980) has limited use of DON as a therapeutic agent, and DON prodrugs with reduced toxicity are in development. Regardless, because the immune system plays a role in both CNS pathology and virus clearance, thoughtful consideration should be employed when evaluating drugs that suppress the immune system as potential therapeutics for alphavirus encephalomyelitis.

## Acknowledgements

The authors would like to thank Joseph Mankowski for the use of his microscope and StereoInvestigator software and Kelly Metcalf Pate, Lisa Mangus, Elizabeth Troisi, Jane Xie, and Robert Mathey for technical assistance. This work was supported by grants from the US National Institutes of Health: R01 NS038932 (DEG) and T32 8T32OD11089 (VKB), and the AVMA Externship Stipend Program (AMB).

## References

Akaoka, H., Szymocha, R., Beurton-Marduel, P., Bernard, A., Belin, M.F., Giraudon, P., 2001. Functional changes in astrocytes by human T-lymphotropic virus type-1 T-lymphocytes. Virus Res. 78, 57–66.
Alt, J., Potter, M.C., Rojas, C., Slusher, B.S., 2015. Bioanalysis of 6-diazo-5-oxo-l-norleucine in plasma and brain by ultra-performance liquid chromatography mass spectrometry. Anal. Biochem. 474, 28–34.
Babi, M.A., Raleigh, T., Shapiro, R.E., McSherry, J., Applebee, A., 2014. MRI and encephalography in fatal eastern equine encephalitis. Neurology 83, 1483, (1483).
Baig, B., Mehta, T., Khalid, N., Chhabra, L., 2014. Eastern equine encephalitis: a classical case. Conn. Med. 78, 529–531.
Baxter, V.K., Griffin, D.E., 2016. Interferon gamma modulation of disease manifestation and the local antibody response to alphavirus encephalomyelitis. J. Gen. Virol. 97, 2908–2925.
Binder, G.K., Griffin, D.E., 2001. Interferon-gamma -mediated site-specific clearance of alphavirus from CNS neurons. Science 293, 303–306.
Biron, C.A., Turgiss, L.R., Welsh, R.M., 1983. Increase in NK cell number and turnover rate during acute viral infection. J. Immunol. 131, 1539–1545.
Brison, E., Jacomy, H., Desforges, M., Talbot, P.J., 2011. Glutamate excitotoxicity Is involved in the induction of paralysis in mice after infection by a human coronavirus with a single point mutation in its spike protein. J. Virol. 85, 12464–12473.
Bruyn, H.B., Lennette, E.H., 1953. Western equine encephalitis in infants; a report on three cases with sequelae. Calif. Med. 79, 362–366.
Burdeinick-Kerr, R., Wind, J., Griffin, D.E., 2007. Synergistic roles of antibody and interferon in noncytolytic clearance of Sindbis virus from different regions of the central nervous system. J. Virol. 81, 5628–5636.
Byrnes, A.P., Durbin, J.E., Griffin, D.E., 2000. Control of Sindbis virus infection by antibody in interferon-deficient mice. J. Virol. 74, 3905–3908.
Carpentier, P.A., Begolka, W.S., Olson, J.K., Elhofy, A., Karpus, W.J., Miller, S.D., 2004. Differential activation of astrocytes by innate and adaptive immune stimuli. Glia 49, 360–374.
Carr, E.L., Kelman, A., Wu, G.S., Gopaul, R., Senkevitch, E., Aghvanyan, A., Turay, A.M., Frauwirth, K.A., 2010. Glutamine uptake and metabolism are coordinately regulated by ERK/MAPK during T lymphocyte activation. J. Immunol. 185, 1037–1044.
Carriedo, S.G., Sensi, S.L., Yin, H.Z., Weiss, J.H., 2000. AMPA exposures induce mitochondrial Ca(2+) overload and ROS generation in spinal motor neurons in vitro. J. Neurosci. 20, 240–250.
Colombo, S.L., Palacios-Callender, M., Frakich, N., De Leon, J., Schmitt, C.A., Boorn, L., Davis, N., Moncada, S., 2010. Anaphase-promoting complex/cyclosome-Cdh1 coordinates glycolysis and glutaminolysis with transition to S phase in human T lymphocytes. Proc. Natl. Acad. Sci. USA 107, 18868–18873.
Conrady, C.D., Drevets, D.A., Carr, D.J.J., 2010. Herpes simplex type I (HSV-1) infection of the nervous system: is an immune response a good thing? J. Neuroimmunol. 220, 1–9.
Danbolt, N.C., 2001. Glutamate uptake. Prog. Neurobiol. 65, 1–105.
Darman, J., Backovic, S., Dike, S., Maragakis, N.J., Krishnan, C., Rothstein, J.D., Irani, D.N., Kerr, D.A., 2004. Viral-Induced Spinal Motor Neuron Death Is Non-Cell-Autonomous and Involves Glutamate Excitotoxicity. J. Neurosci. 24, 7566–7575.
Darwich, L., Coma, G., Pena, R., Bellido, R., Blanco, E.J.J., Este, J.A., Borras, F.E., Clotet, B., Ruiz, L., Rosell, A., Andreo, F., Parkhouse, R.M.E., Bofill, M., 2009. Secretion of interferon-gamma by human macrophages demonstrated at the single-cell level after costimulation with interleukin (IL)−12 plus IL-18. Immunology 126, 383–393.
Deresiewicz, R.L., Thaler, S.J., Hsu, L., Zamani, A.A., 1997. Clinical and neuroradiographic manifestations of eastern equine encephalitis. N. Engl. J. Med. 336, 1867–1874.
Dokun, A.O., Kim, S., Smith, H.R.C., Kang, H.-S.P., Chu, D.T., Yokoyama, W.M., 2001. Specific and nonspecific NK cell activation during virus infection. Nat. Immunol. 2, 951–956.
Earhart, R.H., Amato, D.J., Chang, A.Y., Borden, E.C., Shiraki, M., Dowd, M.E., Comis, R.L., Davis, T.E., Smith, T.J., 1990. Phase II trial of 6-diazo-5-oxo-L-norleucine versus aclacinomycin-A in advanced sarcomas and mesotheliomas. Invest. New Drugs 8, 113–119.
Earhart, R.H., Koeller, J.M., Davis, H.L., 1982. Phase I trial of 6-diazo-5-oxo-L-norleucine (don) administered by 5-day courses. Cancer Treat. Rep. 66, 1215–1217.
Eng, L.F., Ghirnikar, R.S., 1994. GFAP and astrogliosis. Brain Pathol. 4, 229–237.
Ethier, M., Rogg, J., 2012. Eastern equine encephalitis: MRI findings in two patients. Med. Health R I 95, 227–229.
Finley, K.H., Longshore, W.A., Palmer, R.J., Cook, R.E., Riggs, N., 1955. Western equine and St. Louis encephalitis; preliminary report of a clinical follow-up study in California. Neurology 5, 223–235.
Gardiner, C.M., Finlay, D.K., 2017. What fuels natural killers? Metabolism and NK cell responses. Front. Immunol. 8, 367.
Go, Y.Y., Balasuriya, U.B.R., Lee, C.-K., 2014. Zoonotic encephalitides caused by arboviruses: transmission and epidemiology of alphaviruses and flaviviruses. Clin. Exp. Vaccin. Res. 3, 58, (20).
Gordon, E.B., Hart, G.T., Tran, T.M., Waisberg, M., Akkaya, M., Kim, A.S., Hamilton, S.E., Pena, M., Yazew, T., Qi, C.-F., Lee, C.-F., Lo, Y.-C., Miller, L.H., Powell, J.D., Pierce, S.K., 2015. Targeting glutamine metabolism rescues mice from late-stage cerebral malaria. Proc. Natl. Acad. Sci. USA 112, 13075–13080.
Greene, I.P., Lee, E.-Y., Prow, N., Ngwang, B., Griffin, D.E., 2008. Protection from fatal viral encephalomyelitis: ampa receptor antagonists have a direct effect on the inflammatory response to infection. Proc. Natl. Acad. Sci. USA 105, 3575–3580.
Griffin, D.E., 2011. Viral Encephalomyelitis. PLoS Pathog. 7, e1002004.
Griffin, D.E., 2003. Immune responses to RNA-virus infections of the CNS. Nat. Rev. Immunol. 3, 493–502.
Harvala, H., Bremner, J., Kealey, S., Weller, B., McLellan, S., Lloyd, G., Staples, E., Faggian, F., Solomon, T., 2009. Case report: eastern equine encephalitis virus imported to the UK. J. Med. Virol. 81, 305–308.
Havert, M.B., Schofield, B., Griffin, D.E., Irani, D.N., 2000. Activation of divergent neuronal cell death pathways in different target cell populations during neuroadapted Sindbis virus infection of mice. J. Virol. 74, 5352–5356.
Ito, D., Imai, Y., Ohsawa, K., Nakajima, K., Fukuuchi, Y., Kohsaka, S., 1998. Microglia-specific localisation of a novel calcium binding protein, Iba1. Brain Res. Mol. Brain Res. 57, 1–9.
Jackson, A.C., Moench, T.R., Trapp, B.D., Griffin, D.E., 1988. Basis of neurovirulence in Sindbis virus encephalomyelitis of mice. Lab. Invest. 58, 503–509.
Jiang, Z.G., Piggee, C., Heyes, M.P., Murphy, C., Quearry, B., Bauer, M., Zheng, J., Gendelman, H.E., Markey, S.P., 2001. Glutamate is a mediator of neurotoxicity in secretions of activated HIV-1-infected macrophages. J. Neuroimmunol. 117, 97–107.
Kimura, T., Griffin, D.E., 2003. Extensive immune-mediated hippocampal damage in mice surviving infection with neuroadapted Sindbis virus. Virology 311, 28–39.
Koutsilieri, E., Sopper, S., Heinemann, T., Scheller, C., Lan, J., Stahl-Hennig, C., Meulen, ter, V., Riederer, P., Gerlach, M., 1999. Involvement of microglia in cerebrospinal fluid glutamate increase in SIV-infected rhesus monkeys (Macaca mulatta). AIDS Res. Hum. Retrovir. 15, 471–477.
Kulcsar, K.A., Baxter, V.K., Abraham, R., Nelson, A., Griffin, D.E., 2015. Distinct immune responses in resistant and susceptible strains of mice during neurovirulent alphavirus encephalomyelitis. J. Virol. 89, 8280–8291.
Kulcsar, K.A., Baxter, V.K., Greene, I.P., Griffin, D.E., 2014. Interleukin 10 modulation of

pathogenic Th17 cells during fatal alphavirus encephalomyelitis. Proc. Natl. Acad. Sci. USA 111, 16053–16058.
Lee, C.-F., Lo, Y.-C., Cheng, C.-H., Furtmüller, G.J., Oh, B., Andrade-Oliveira, V., Thomas, A.G., Bowman, C.E., Slusher, B.S., Wolfgang, M.J., Brandacher, G., Powell, J.D., 2015. Preventing allograft rejection by targeting immune metabolism. Cell Rep. 13, 760–770.
Lee, J.M., Zipfel, G.J., Choi, D.W., 1999. The changing landscape of ischaemic brain injury mechanisms. Nature 399, A7–A14.
Levine, B., Hardwick, J.M., Trapp, B.D., Crawford, T.O., Bollinger, R.C., Griffin, D.E., 1991. Antibody-mediated clearance of alphavirus infection from neurons. Science 254, 856–860.
Lewis, J., Oyler, G.A., Ueno, K., Fannjiang, Y.R., Chau, B.N., Vornov, J., Korsmeyer, S.J., Zou, S., Hardwick, J.M., 1999. Inhibition of virus-induced neuronal apoptosis by Bax. Nat. Med. 5, 832–835.
Lewis, J., Wesselingh, S.L., Griffin, D.E., Hardwick, J.M., 1996. Alphavirus-induced apoptosis in mouse brains correlates with neurovirulence. J. Virol. 70, 1828–1835.
Lopez-Verges, S., Milush, J.M., Schwartz, B.S., Pando, M.J., Jarjoura, J., York, V.A., Houchins, J.P., Miller, S., Kang, S.-M., Norris, P.J., Nixon, D.F., Lanier, L.L., 2011. Expansion of a unique CD57+NKG2Chi natural killer cell subset during acute human cytomegalovirus infection. Proc. Natl. Acad. Sci. USA 108, 14725–14732.
Lubelczyk, C., Mutebi, J.P., Robinson, S., Elias, S.P., Smith, L.B., Juris, S.A., Foss, K., Lichtenwalner, A., Shively, K.J., Hoenig, D.E., Webber, L., Sears, S., Smith, R.P., 2013. An epizootic of eastern equine encephalitis virus, Maine, USA in 2009: outbreak description and entomological studies. Am. J. Trop. Med. Hyg. 88, 95–102.
Lury, K., Castillo, M., 2004. Eastern equine encephalitis: ct and MRI findings in one case. Emerg. Radiol. 11, 46–48.
Lustig, S., Jackson, A.C., Hahn, C.S., Griffin, D.E., Strauss, E.G., Strauss, J.H., 1988. Molecular basis of Sindbis virus neurovirulence in mice. J. Virol. 62, 2329–2336.
Maciolek, J.A., Pasternak, J.A., Wilson, H.L., 2014. Metabolism of activated T lymphocytes. Curr. Opin. Immunol. 27, 60–74.
Magill, G.B., Myers, W., Reilly, H.C., Putnam, R.C., 1957. Pharmacological and initial therapeutic observations on 6-Diazo-5-Oxo-L-Norleucine (Don) in human neoplastic disease. Cancer 10, 1138–1150.
Mancao, M.Y., Imran, H., Chandra, S., Estrada, B., Figarola, M., Sosnowski, J., Vidal, R., 2009. Eastern equine encephalitis virus infeciton and hemophagocytic lymphohistiocytosis in a 5-month-old infant. Pediatr. Infect. Dis. J. 28, 543–545.
Manivannan, S., Baxter, V.K., Schultz, K.L.W., Slusher, B.S., Griffin, D.E., 2016. Protective effects of glutamine antagonist 6-diazo-5-oxo-l-norleucine in mice with alphavirus encephalomyelitis. J. Virol. 90, 9251–9262.
Mishra, M.K., Koli, P., Bhowmick, S., Basu, A., 2007. Neuroprotection conferred by astrocytes is insufficient to protect animals from succumbing to Japanese encephalitis. Neurochem. Int. 50, 764–773.
Mishra, M.K., Kumawat, K.L., Basu, A., 2008. Japanese encephalitis virus differentially modulates the induction of multiple pro-inflammatory mediators in human astrocytoma and astroglioma cell-lines. Cell Biol. Int. 32, 1506–1513.
Molaei, G., Armstrong, P.M., Graham, A.C., Kramer, L.D., Andreadis, T.G., 2015. Insights into the recent emergence and expansion of eastern equine encephalitis virus in a new focus in the Northern New England USA. Parasit. Vectors e8, 516.
Nadler, J.V., Perry, B.W., Cotman, C.W., 1978. Intraventricular kainic acid preferentially destroys hippocampal pyramidal cells. Nature 271, 676–677.
Nargi-Aizenman, J.L., Havert, M.B., Zhang, M., Irani, D.N., Rothstein, J.D., Griffin, D.E., 2004. Glutamate receptor antagonists protect from virus-induced neural degeneration. Ann. Neurol. 55, 541–549.
Newsholme, E.A., Crabtree, B., Ardawi, M.S., 1985. Glutamine metabolism in lymphocytes: its biochemical, physiological and clinical importance. Q. J. Exp. Physiol. 70, 473–489.
Nicotera, P., Orrenius, S., 1998. The role of calcium in apoptosis. Cell Calcium 23, 173–180.
Olney, J.W., Fuller, T., de Gubareff, T., 1979. Acute dendrotoxic changes in the hippocampus of kainate treated rats. Brain Res. 176, 91–100.
Ovanesov, M.V., Vogel, M.W., Moran, T.H., Pletnikov, M.V., 2007. Neonatal Borna disease virus infection in rats is associated with increased extracellular levels of glutamate and neurodegeneration in the striatum. J. Neurovirol. 13, 185–194.
Persson, M., Brantefjord, M., Liljeqvist, J.-Å., Bergström, T., Hansson, E., Rönnbäck, L., 2007. Microglial GLT-1 is upregulated in response to herpes simplex virus infection to provide an antiviral defence via glutathione. Glia 55, 1449–1458.
Plaimas, K., Wang, Y., Rotimi, S.O., Olasehinde, G., Fatumo, S., Lanzer, M., Adebiyi, E., König, R., 2013. Computational and experimental analysis identified 6-diazo-5-oxonorleucine as a potential agent for treating infection by Plasmodium falciparum. Infect. Genet. Evol. 20, 389–395.
Potter, M.C., Baxter, V.K., Mathey, R.W., Alt, J., Rojas, C., Griffin, D.E., Slusher, B.S., 2015. Neurological sequelae induced by alphavirus infection of the CNS are attenuated by treatment with the glutamine antagonist 6-diazo-5-oxo-l-norleucine. J. Neurovirol. 21, 159–173.
Prow, N.A., Irani, D.N., 2008. The inflammatory cytokine, interleukin-1 beta, mediates loss of astroglial glutamate transport and drives excitotoxic motor neuron injury in the spinal cord during acute viral encephalomyelitis. J. Neurochem. 105, 1276–1286.
Prow, N.A., Irani, D.N., 2007. The opioid receptor antagonist, naloxone, protects spinal motor neurons in a murine model of alphavirus encephalomyelitis. Exp. Neurol. 205, 461–470.
Przelomski, M.M., O'Rourke, E., Grady, G.F., Berardi, V.P., Markley, H.G., 1988. Eastern equine encephalitis in Massachusetts: a report of 16 cases, 1970–1984. Neurology 38, 736–739.
Rais, R., Jančařík, A., Tenora, L., Nedelcovych, M., Alt, J., Englert, J., Rojas, C., Le, A., Elgogary, A., Tan, J., Monincová, L., Pate, K., Adams, R., Ferraris, D., Powell, J., Majer, P., Slusher, B.S., 2016. Discovery of 6-Diazo-5-oxo- l-norleucine (DON) prodrugs with enhanced CSF delivery in monkeys: a potential treatment for glioblastoma. J. Med. Chem. 59, 8621–8633.
Reddy, A.J., Woods, C.W., Welty-Wolf, K.E., 2008. Eastern equine encephalitis leading to multi-organ failure and sepsis. J. Clin. Virol. 42, 418–421.
Rivas, F., Diaz, L.A., Cardenas, V.M., Daza, E., Bruzon, L., Alcala, A., la Hoz, De, O., Caceres, F.M., Aristizabal, G., Martinez, J.W., Revelo, D., la Hoz, De, F., Boshell, J., Camacho, T., Calderon, L., Olano, V.A., Villarreal, L.I., Roselli, D., Alvarez, G., Ludwig, G., Tsai, T., 1997. Epidemic Venezuelan equine encephalitis in La Guajira, Colombia, 1995. J. Infect. Dis. 175, 828–832.
Rothstein, J.D., Jin, L., Dykes-Hoberg, M., Kuncl, R.W., 1993. Chronic inhibition of glutamate uptake produces a model of slow neurotoxicity. Proc. Natl. Acad. Sci. USA 90, 6591–6595.
Rothstein, J.D., Martin, L., Levey, A.I., Dykes-Hoberg, M., 1994. Localization of neuronal and glial glutamate transporters. Neuron 13, 713–725.
Rowell, J.F., Griffin, D.E., 2002. Contribution of T cells to mortality in neurovirulent Sindbis virus encephalomyelitis. J. Neuroimmunol. 127, 106–114.
Rowell, J.F.J., Griffin, D.E.D., 1999. The inflammatory response to nonfatal Sindbis virus infection of the nervous system is more severe in SJL than in BALB/c mice and is associated with low levels of IL-4 mRNA and high levels of IL-10-producing CD4+ T cells. J. Immunol. 162, 1624–1632.
Rozdilsky, B., Robertson, H.E., Chorney, J., 1968. Western encephalitis: report of eight fatal cases. Saskatchewan epidemic, 1965. Can. Med. Assoc. J. 98, 79–86.
Sattler, R., Tymianski, M., 2001. Molecular mechanisms of glutamate receptor-mediated excitotoxic neuronal cell death. Mol. Neurobiol. 24, 107–129.
Schultz, D.R., Barthal, J.S., Garrett, G., 1977. Western equine encephalitis with rapid onset of parkinsonism. Neurology 27, 1095–1096.
Shelton, L.M., Huysentruyt, L.C., Seyfried, T.N., 2010. Glutamine targeting inhibits systemic metastasis in the VM-M3 murine tumor model. Int. J. Cancer 127, 2478–2485.
Shijie, J., Takeuchi, H., Yawata, I., Harada, Y., Sonobe, Y., Doi, Y., Liang, J., Hua, L., Yasuoka, S., Zhou, Y., Noda, M., Kawanokuchi, J., Mizuno, T., Suzumura, A., 2009. Blockade of glutamate release from microglia attenuates experimental autoimmune encephalomyelitis in mice. Tohoku J. Exp. Med. 217, 87–92.
Sklaroff, R.B., Casper, E.S., Magill, G.B., Young, C.W., 1980. Phase I study of 6-diazo-5-oxo-L-norleucine (DON). Cancer Treat. Rep. 64, 1247–1251.
Sullivan, M.P., Nelson, J.A., Feldman, S., Van Nguyen, B., 1988. Pharmacokinetic and phase I study of intravenous DON (6-diazo-5-oxo-L-norleucine) in children. Cancer Chemother. Pharmacol. 21, 78–84.
Sun, J.C., Bellke, J.N., Lanier, L.L., Takeuchi, H., 2009. Adaptive immune features of natural killer cells. Nature 457, 557–561.
Sun, J.C., Lanier, L.L., 2011. NK cell development, homeostasis and function: parallels with CD8+ T cells. Nat. Rev. Immunol. 11, 645–657.
Takeuchi, H., Suzumura, A., 2014. Gap junctions and hemichannels composed of connexinsconnexins: potential therapeutic targets for neurodegenerative diseases. Front. Cell. Neurosic. e8, 189.
Thangavelu, K., Chong, Q.Y., Low, B.C., Sivaraman, J., 2014. Structural basis for the active site inhibition mechanism of human kidney-type glutaminase (KGA). Sci. Rep. 4, 3827.
Tilleux, S., Hermans, E., 2007. Neuroinflammation and regulation of glial glutamate uptake in neurological disorders. J. Neurosci. Res. 85, 2059–2070.
Trinchieri, G., Matsumoto-Kobayashi, M., Clark, S.C., Seehra, J., London, L., Perussia, B., 1984. Response of resting human peripheral blood natural killer cells to interleukin 2. J. Exp. Med. 160, 1147–1169.
Vilcarromero, S., Aguilar, P.V., Halsey, E.S., V., Laguna-Torres, A., Razuri, H., Perez, J., Valderrama, Y., Gotuzzo, E., Suárez, L., Céspedes, M., Kochel, T.J., 2010. Venezuelan equine encephalitis and two human deaths, Peru. Emerg. Infect. Dis. 16, 553–556.
Wang, R., Dillon, C.P., Shi, L.Z., Milasta, S., Carter, R., Finkelstein, D., McCormick, L.L., Fitzgerald, P., Chi, H., Munger, J., Green, D.R., 2011. The transcription factor Myc controls metabolic reprogramming upon T lymphocyte activation. Immunity 35, 871–882.
Weaver, S.C., Salas, R., Rico-Hesse, R., Ludwig, G.V., Oberste, M.S., Boshell, J., Tesh, R.B., 1996. Re-emergence of epidemic Venezuelan equine encephalomyelitis in South America. VEE Study Group. Lancet 348, 436–440.
Zhang, L., Li, L., Wang, B., Qian, D.-M., Song, X.-X., Hu, M., 2014. HCMV induces dysregulation of glutamate uptake and transporter expression in human fetal astrocytes. Neurochem. Res. 39, 2407–2418.